ACCSCIENCE PUBLISHING

International Journal of Bioprinting

REVIEW ARTICLE

State-of-the-art research progress and emerging strategies in digital light processing bioprinting for skin regeneration

Fowzul Islam Fahad[1], Minjun Ahn[2], and Byoung Soo Kim[1,2,3]*

[1]Department of Biomedical Convergence Engineering, School of Biomedical Convergence Engineering, Pusan National University, Yangsan, Gyeongsangnam-do, Republic of Korea

[2]Medical Research Institute, Pusan National University, Yangsan, Gyeongsangnam-do, Republic of Korea

[3]Research Institute for Convergence of Biomedical Science and Technology, Pusan National University Yangsan Hospital, Yangsan, Gyeongsangnam-do, Republic of Korea

Abstract

Skin injuries, including burns, chronic wounds, and diabetic ulcers, present significant clinical challenges due to impaired healing, high risk of infection, and limited efficacy of conventional transdermal patches. Owing to recent advances in biomaterials and regenerative medicine, skin-repair strategies are currently focused on engineered patches that better mimic the native tissue structure and function. In particular, digital light processing (DLP)-based 3D printing is a powerful platform for fabricating high-resolution, personalized skin patches with precise architectural control compared to conventional approaches. The rapid layer-by-layer photopolymerization of hydrogel-based materials enables the creation of mechanically compliant biocompatible constructs that support cell proliferation, immunomodulation, angiogenesis, and extracellular matrix remodeling. Furthermore, DLP technology enables controlled therapeutic delivery by facilitating the integration of advanced functionalities, such as microneedle arrays, vascularized architectures, and stimuli-responsive systems. This review systematically discusses the fundamental principles of DLP printing, key parameters that govern printing fidelity, recent progress in bioink development, and emerging applications of DLP-fabricated skin patches in wound healing and skin regeneration. Additionally, current challenges and future perspectives are highlighted to guide the continued development and clinical translation of DLP-based regenerative skin therapies.

Keywords: Digital light processing; 3D printing; Transdermal drug delivery; Personalized patches; Skin regeneration; Wound healing

***Corresponding author:**
Byoung Soo Kim
(bskim7@pusan.ac.kr)

Citation: Fahad FI, Ahn M, Kim BS. State-of-the-art research progress and emerging strategies in digital light processing bioprinting for skin regeneration. *Int J Bioprint.* 2026;12(4):026220217. doi: 10.36922/IJB026220217

Received: May 26, 2026

Revised: June 24, 2026

Accepted: June 26, 2026

Published online: June 29, 2026

1. Introduction

The skin is the largest organ of the body and functions as a highly organized and multifunctional biological system that directly interfaces with the external environment. It comprises a complex assembly of structural proteins (e.g., collagen and elastin), cells, various plasma proteins and polypeptide constituents, and a substantial fraction of water to form a matrix, within which is embedded an extensive network of nerve fibers, blood

vessels, and lymphatic nodes that support physiological signaling, nutrient exchange, and immune cell infiltration.[1,2] Critically, this matrix is not architecturally uniform but is organized into three hierarchically distinct layers—the epidermis, dermis, and subcutaneous tissue—each characterized by unique cell populations, extracellular matrix (ECM) compositions, and mechanical properties that collectively enable the skin's integrated functions, including mechanical strength, elasticity, metabolic activity, sensory capability, and physiological activity, to sustain overall physiological homeostasis through barrier protection, thermoregulation, immunological defense, and the perception of environmental stimuli.[3-5] However, injuries such as burns, chronic wounds, diabetic ulcers, and surgical trauma severely compromise this protective, multi-layered organ, causing delayed tissue repair, high risk of infection, and substantial socioeconomic impact.[6,7] Traditional wound management strategies, such as gauze dressings and topical ointments, are limited in their ability to provide a moist environment, promote cellular migration, and precisely deliver bioactive agents. Critically, they are entirely incapable of reproducing the stratified, hierarchical organization of native skin. These limitations often result in prolonged healing times, scarring, and poor functional recovery.[8-10] Recent progress in biomedical engineering in the development of advanced biomaterials, such as natural polymers, synthetic hydrogels, and decellularized ECM (dECM)-based bioinks that offer tunable mechanics, biocompatibility, and controlled release of bioactive agents, has catalyzed a regenerative approach for skin repair.[11-14] Nevertheless, conventional scaffold fabrication techniques used to process these biomaterials, including solvent casting, freeze-drying, and electrospinning, typically yield compositionally uniform constructs with limited spatial resolution and control, rendering them insufficient to replicate the discrete mechanical and biochemical gradients present across the epidermal, dermal, and subcutaneous strata of native skin. Three-dimensional (3D) printing has emerged to overcome these structural limitations by enabling spatially defined, layer-by-layer material deposition, allowing independent engineering of compositionally and mechanically distinct zones within a single construct that more faithfully mimic the native multi-layered skin architecture. Accordingly, these advanced biomaterials have been increasingly coupled with 3D printing technologies to advance therapeutic strategies by enabling precise, customizable fabrication of transdermal patches and skin substitutes that closely mimic the native ECM architecture for promoting tissue regeneration and improving the effectiveness of engineered skin patches.[15-17]

Among the available 3D printing modalities, digital light processing (DLP) is a vat photopolymerization-based technique that is currently gaining significant attention for the fabrication of advanced skin patches, owing to distinct advantages over conventional 3D printing approaches. Conventional bioprinting approaches possess several inherent limitations that restrict their ability to recapitulate the complex microstructure of native skin. For example, extrusion-based bioprinting, the most widely used technique, is constrained by relatively low printing resolution (typically 200–500 μm), shear-induced stress on encapsulated cells and bioactive agents, and limited capability to reproduce fine microscale features. Similarly, inkjet bioprinting enables high-throughput deposition of low-viscosity bioinks but suffers from nozzle clogging, restricted material compatibility, and insufficient mechanical robustness of the resulting constructs. Although stereolithography (SLA) affords high fabrication precision, its point-wise laser scanning constrains throughput for large or complex constructs, while extended photopolymerization exposure can adversely affect cell viability and compromise the integrity of fragile biomolecules. In contrast, DLP uses a digital micromirror device (DMD) to simultaneously cure entire layers of photosensitive material.[18,19] This approach accelerates the fabrication process (up to 1 mm^3/s) while reducing mechanical stresses on the material. This process results in smoother surfaces that minimize irritation and enhance cell viability and biochemical stability, which are essential for skin-contact applications. DLP-based patches are often infused with hydrogel networks to create a hydrated biocompatible microenvironment that promotes cell proliferation, angiogenesis, and ECM remodeling in skin tissue regeneration.[20-22] Moreover, DLP shows versatility in fabricating various products such as microneedle (MN) arrays, vascularized constructs, stimuli-responsive dressings, and theranostic biomedical patches, which improve the efficiency and precision of drug delivery and integrate functionalities that support the various stages of wound healing in skin patches for notably superior skin regeneration.[23-25]

2. Objective and methodology

This review aims to provide a comprehensive analysis of DLP-based skin patches and drug delivery techniques for skin regenerative applications. It systematically examines the fundamental printing mechanisms underlying DLP technology, with particular emphasis on light-mediated photopolymerization and factors influencing structural fidelity and resolution, and summarizes recent innovations in bioink development, especially the advancement of bioactive and functionalized hydrogel systems designed for enhanced skin regeneration. In addition, emerging

therapeutic delivery strategies integrated within DLP-fabricated constructs are evaluated, highlighting controlled drug release, immunomodulation, and multifunctional patch design for skin regeneration. The systematic literature search was performed across PubMed, Google Scholar, and the Cochrane Library to identify peer-reviewed articles. The search included keywords such as transdermal patches, transdermal drug delivery, DLP bioprinting scaffolds, wound healing, diabetic wound healing, skin regeneration, bioinspired patches, DLP-based drug delivery, and stimuli-responsive drug delivery. Boolean operators (AND, OR) were used to refine the search strategy. Studies were included if they evaluated (i) DLP-based transdermal patch fabrication and (ii) DLP-based transdermal patches for skin regeneration (e.g., wound healing, diabetic wound healing, psoriasis, atopic dermatitis, acne vulgaris) applications.

3. Design requirements of regenerative skin patches

The development of regenerative skin patches requires a comprehensive understanding of the structural, mechanical, biological, and functional characteristics of native skin. Unlike conventional wound dressings that primarily provide physical protection, advanced regenerative patches are designed to actively participate in the healing process by recreating key features of the native tissue microenvironment. Given the hierarchical organization and multifunctional nature of skin, successful regenerative systems must integrate biomimetic architectures, appropriate mechanical properties, controlled biological signaling, and responsive functionalities to support tissue reconstruction and functional restoration.[26,27]

3.1. Structural, mechanical, and morphological requirements

Skin is a highly organized, multilayered organ consisting of the epidermis, dermis, and hypodermis, each characterized by distinct cellular compositions, ECM organizations, and physiological functions. Therefore, regenerative skin patches should be designed to mimic the hierarchical architecture and physicochemical gradients present within native skin.[5,28]

A critical structural requirement is the incorporation of an interconnected porous network capable of facilitating cell infiltration, nutrient transport, oxygen diffusion, and metabolic waste removal. Scaffold porosity significantly influences cellular behavior and tissue regeneration. Previous studies have demonstrated that pore sizes ranging from 5–15 μm support fibroblast infiltration, and those between 20–125 μm facilitate dermal tissue regeneration. Furthermore, gradient pore architectures have attracted considerable attention because they more closely replicate the heterogeneous microenvironment of native skin and provide spatial cues that enhance cellular migration, tissue integration, and re-epithelialization. In another study, high scaffold porosity (greater than 60%) was shown to enhance skin regeneration by improving nutrient supply and oxygen diffusion. Moreover, maintaining a moist environment is essential for promoting cell infiltration and supporting nutrient transport between the wound bed and the scaffold, both of which are strongly influenced by pore size and porosity.[29-32]

The mechanical properties of regenerative skin patches play a fundamental role in determining their clinical performance and biological functionality. Native skin exhibits viscoelastic behavior, allowing it to undergo continuous deformation while maintaining structural integrity. Therefore, engineered skin substitutes should possess mechanical properties that closely match those of the surrounding tissue. The elastic modulus of healthy human skin typically ranges between 4.5 and 8 kPa, although considerable variation exists depending on anatomical location and age. Scaffolds exhibiting comparable mechanical characteristics are better able to withstand physiological stresses while maintaining intimate contact with the wound surface. Mechanical mismatch between implanted materials and host tissue can impair cellular integration, induce inflammation, and compromise healing outcomes. Beyond simple mechanical matching, increasing evidence suggests that cells actively respond to the stiffness of their surrounding microenvironment through mechanotransduction pathways. This phenomenon, known as durotaxis, describes the tendency of cells such as fibroblasts, keratinocytes, and endothelial cells to migrate along stiffness gradients. Moreover, several studies have shown that direct contact with the wound bed and the topographical cues of engineered patches can induce mechanobiological pathway activation, thereby promoting skin regeneration more effectively than flat, film-like structures. Therefore, incorporating controlled mechanical gradients with balanced pore size and porosity into regenerative patches may provide a powerful strategy for directing nutrient infiltration, cellular migration, tissue organization, and wound closure.[31-34]

3.2. Biological and functional regulation

Beyond providing structural support, regenerative skin patches should actively regulate the biological processes associated with wound healing. Tissue regeneration is orchestrated through complex interactions among cells, growth factors, cytokines, and ECM components.[35,36] Consequently, advanced biomaterials increasingly

function as bioactive platforms capable of delivering biological signals through controlled therapeutic delivery. Skin tissue regeneration involves a complex cascade of cellular and biochemical events, and chronic or impaired conditions may result from the dysregulation of these biological activities. Skin patches incorporating exogenous growth factors and cytokines can effectively guide cellular behavior and enhance tissue repair. Key growth factors, including vascular endothelial growth factor (VEGF), fibroblast growth factor (FGF), and platelet-derived growth factor (PDGF), play critical roles in angiogenesis, cell proliferation, and tissue remodeling during regeneration. However, successful therapeutic outcomes depend not only on the presence of these biomolecules but also on their precise spatial localization and temporal delivery. Therefore, engineered scaffolds capable of controlled and sustained release are essential to coordinate the complex sequence of events involved in skin tissue regeneration.[29,32,35]

Skin tissue is highly susceptible to microbial invasion and pathogen infection, particularly during the early stages of injury. Therefore, effective elimination of pathogens during the inflammatory phase is essential. However, prolonged or excessive inflammation can impair the healing process and delay tissue regeneration.[37] Consequently, proper immunomodulation is crucial, particularly the transition of macrophages from the pro-inflammatory M1 phenotype to the anti-inflammatory M2 phenotype. Engineered scaffolds should be designed to support this phenotypic shift, thereby promoting a balanced immune response and facilitating efficient skin tissue regeneration. Moreover, damaged skin tissue is associated with a high level of reactive oxygen species (ROS) generation, which can hinder tissue regeneration and prolong the inflammatory phase. Excessive ROS not only causes oxidative stress but is also closely interconnected with the regulation of inflammation and anti-inflammatory responses. Therefore, it is essential to consider these factors in scaffold design to ensure effective ROS scavenging and balanced immunomodulation. Such strategies can help reduce oxidative damage, regulate inflammation, and ultimately enhance skin tissue regeneration.[38-40] Another important factor to consider is hypoxia, which can significantly impair skin tissue regeneration. Oxygen deficiency is a major limitation in chronic and ischemic conditions, where inadequate vascularization compromises tissue survival and regenerative capacity. Therefore, it is crucial to incorporate strategies such as oxygen-releasing particles and hemoglobin-based carriers during the scaffold development for skin regeneration. These approaches can enhance cellular metabolism, promote angiogenesis, and ultimately accelerate tissue regeneration.[41-43]

4. Conventional approaches to skin patch development.

Conventional wound dressings, including gauze, cotton wool, and adhesive bandages, remain the most widely used materials for wound management due to their simplicity, low cost, and accessibility. Their primary function is to provide a physical barrier against microbial contamination while absorbing wound exudates and maintaining basic wound coverage. However, these materials are largely passive and lack the biological and structural functionalities required to actively support tissue regeneration. Furthermore, conventional dressings often exhibit poor conformability to irregular wound geometries and may adhere to newly formed tissue, resulting in pain and secondary tissue damage during removal. Consequently, their ability to facilitate complete skin regeneration remains limited.[44,45] To overcome these limitations, advanced fabrication technologies have been developed to better mimic the native skin microenvironment. Electrospinning has attracted considerable attention because it produces nanofibrous scaffolds that closely resemble the architecture of the ECM, thereby supporting cell adhesion, migration, and proliferation. The high porosity and surface-area-to-volume ratio of electrospun matrices facilitate nutrient exchange and cellular interactions. Nevertheless, electrospinning is primarily suitable for producing thin membrane-like structures and remains limited in its ability to fabricate thick, complex 3D constructs required for full-thickness skin regeneration.[46-48]

To address this, extrusion-based bioprinting is the most widely utilized additive manufacturing technology owing to its versatility and compatibility with a broad range of biomaterials and cell-laden bioinks. The technique enables the deposition of highly viscous materials and supports the fabrication of large-scale tissue constructs. However, extrusion printing is generally constrained by relatively low resolution and slow fabrication speed. In addition, shear stress generated during extrusion can adversely affect cell viability and biological functionality, while nozzle clogging may compromise printing accuracy and reproducibility.[49-51] Similarly, inkjet bioprinting offers rapid and cost-effective fabrication through droplet-based deposition of biomaterials. Although suitable for high-throughput applications, its dependence on low-viscosity bioinks limits material selection and often results in constructs with inadequate mechanical strength and limited structural complexity for advanced skin tissue engineering applications.[52,53] Therefore, light-based fabrication techniques have emerged as promising alternatives for improving printing resolution and structural fidelity. SLA utilizes a focused laser beam to

selectively photopolymerize photosensitive materials and can generate constructs with excellent surface quality and dimensional accuracy. However, because the laser must sequentially scan each point within a layer, the fabrication process is relatively slow, particularly for large or geometrically complex structures. This limitation reduces its practicality for the rapid production of personalized skin substitutes. Moreover, the prolonged exposure to laser irradiation and photopolymerization conditions can negatively affect cell viability and compromise the stability of fragile biomolecules.[54,55]

In contrast, DLP bioprinting has emerged as one of the most promising technologies for skin regeneration owing to its ability to combine high resolution, rapid fabrication, and excellent structural fidelity. Unlike SLA, DLP utilizes a DMD to project patterned light and cure entire layers simultaneously, markedly enhancing fabrication speed (up to 1 mm^3/s) while preserving microscale precision, thereby offering advantages for cell-laden patches and the delivery of fragile biomolecules. Furthermore, the nozzle-free nature of DLP eliminates issues associated with shear-induced cell damage and nozzle clogging, which are commonly observed in extrusion-based systems. The high spatial resolution of DLP enables the fabrication of sophisticated skin-relevant architectures, including multilayer skin constructs, MN arrays, vascularized microchannel networks, and patient-specific wound dressings. Additionally, DLP is highly compatible with photocurable hydrogel-based bioinks, allowing precise control over construct geometry, mechanical properties, and biological functionality. Collectively, these advantages position DLP as a particularly attractive platform for the development of next-generation regenerative skin patches capable of addressing the structural, biological, and functional requirements of skin tissue regeneration.[21,56,57] The comparison of several fabrication processes for skin patches is summarized in Table 1.

5. Fundamentals of digital light processing bioprinting for skin regeneration

5.1. Digital light processing printing setup and mechanism

The setup of a DLP printer is as follows: A DLP apparatus comprises several interdependent components engineered to facilitate precise photopolymerization. The core is a high-resolution light source, typically an ultraviolet (UV) or visible light-emitting diode (LED) projector, integrated with a digital DMD chip that modulates light wavelengths

Table 1. Comparison of skin patch fabrication technologies

Printing technology	Resolution	Printing speed	Cell viability	Bioink compatibility	Structural complexity	Application area
Digital light processing	High (micron-level, down to 10 μm)	Highest (layer-wide projection)	High (nozzle-less system reduces stress)	Photopolymer-based bioinks (GelMA, SilMA, ColMA)	High (complex 3D architectures and micro-features possible)	Soft tissues, micro-structures, vascular constructs, skin patches
Extrusion-based	Low–medium (150–400 μm)	Low–medium (point-by-point path)	Medium to high (though risk of cell lysis due to nozzle pressure)	Widest range of bioinks and viscosities	Limited (higher risk of structural sagging/collapse)	Cartilage, bone, skin tissue
Inkjet-based	Medium–high	High	Medium (potential thermal or mechanical stress)	Low-viscosity inks only (typically 3.5–12 mPa·s)	Limited (due to low viscosity of materials)	Skin, neural tissue
Electrospinning	Sub-micron (fiber level) to micron-scale	Medium (slow accumulation of fiber layers)	High (often acellular; cells usually seeded post-fabrication)	Synthetic and natural polymers (PCL, silk, gelatin)	Limited (primarily 2D mats or thin fibrous films)	ECM mimicry, thin fibrous dressings, unidirectional fluid transport
Wound dressings	N/A	N/A	Generally acellular passive materials	Traditional fibers, gauze, and non-printed polymers	Low (uniform films, meshes, or foam sheets)	Physical barrier, superficial wounds, exudate absorption

Abbreviations: ColMA: Collagen methacrylate; ECM: Extracellular matrix; GelMA: Gelatin methacryloyl; N/A: Not available; PCL: Polycaprolactone; SilMA: Silk fibroin methacrylate.

between 365 and 460 nm to initiate radical polymerization reactions. Next, it contains a photocurable bioink held in a resin vat fabricated from transparent oxygen-permeable materials such as polydimethylsiloxane (PDMS) or fluorinated ethylene propylene (FEP) to ensure uniform light exposure and prevent early curing at the interface. Additionally, a motorized build platform is immersed in the vat and incrementally raised (typically, 25–100 μm per layer) to enable sequential layer formation. The projected light is focused using optical components, such as lenses and mirrors, to enhance resolution. Finally, control software, such as computer-aided design (CAD)-based slicers or custom algorithms, is used to transform the 3D models into binary masks for each layer (Figure 1a).

For biofabrication applications, the DLP system is typically enclosed in a sterile environment to minimize contamination. Furthermore, the bioink is supplemented with photoinitiators (PIs), such as lithium phenyl(2,4,6-trimethylbenzoyl) phosphonate (LAP), and photoabsorbers (PAs), such as tartrazine, to precisely control the curing kinetics and light penetration depth.[4,58]

The printing mechanisms are as follows: The DLP printing mechanism is based on the controlled photopolymerization of bioinks. The incident light initiates free-radical chain reactions to form covalently cross-linked bioink networks (Figure 1c). The first step of the process begins by slicing a digital 3D model (e.g., an STL file of a wound dressing) into two-dimensional (2D) cross sections, where each section represents an individual layer. Then, the DMD projector illuminates the bioink with a patterned light mask, which activates the PIs to generate radicals that react with polymer chains, such as polyethylene glycol diacrylate (PEGDA) (Figure 1d). This process solidifies the layer within seconds (typically, 1–10 s). The second step involves the printed layer remaining attached to the build platform. In the third step, the build platform rises after each layer cures, allowing uncured bioink to flow into the voids via capillary action or mechanical agitation. This ensures uniform layer formation, and it prevents defects such as delamination or voids. This cycle is repeated until the complete structure is formed (Figure 1b).[58,59] The post-processing steps include solvent rinsing to remove residual monomers, additional secondary UV curing applied to enhance crosslink density, and lyophilization to modulate porosity and further refine the construct.[60]

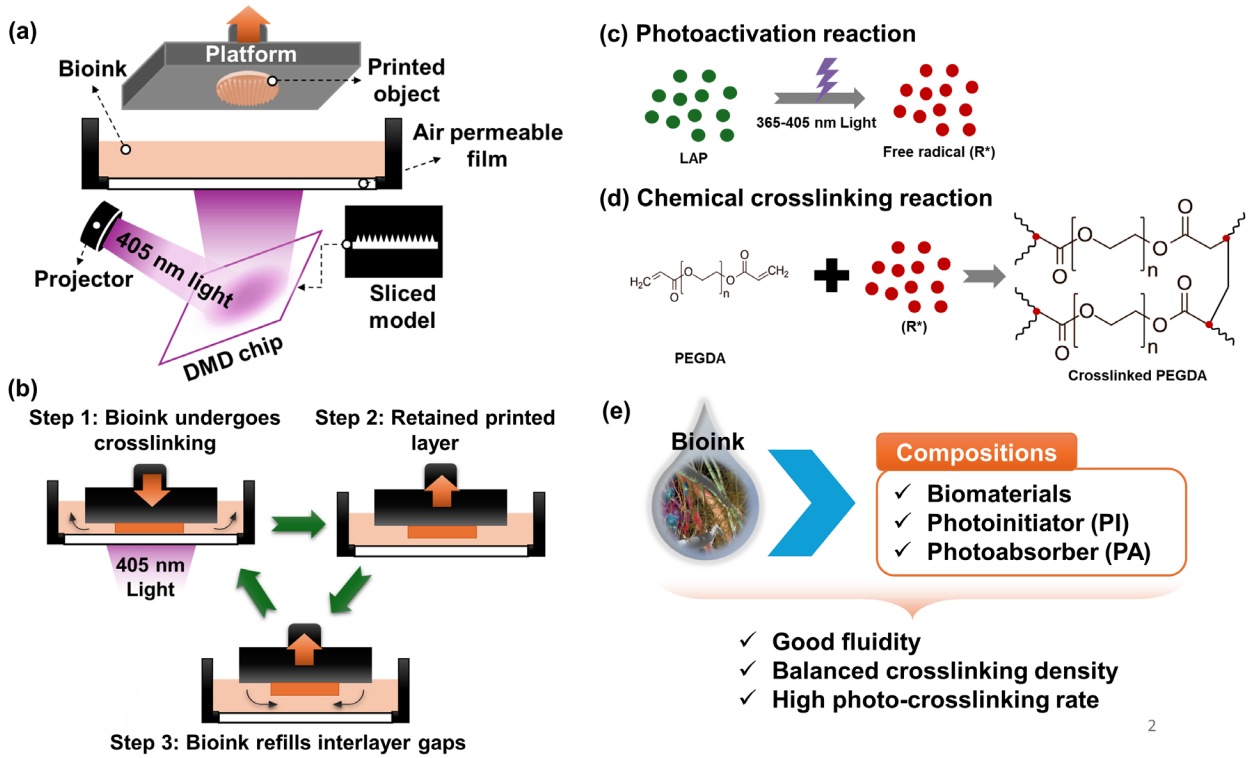

Figure 1. Overview of digital light processing (DLP) bioprinting platform, photopolymerization, and bioink characteristics. (a) DLP printer setup. (b) Schematic representation of the printing mechanism (arrow indicates the flow behavior of bioink). (c) Photoactivation mechanism of the photoinitiator. (d) Chemical crosslinking reaction mechanism. (e) Basic characteristics of a bioink for DLP printing.
Abbreviations: DMD: Digital micromirror device; LAP: Lithium phenyl(2,4,6-trimethylbenzoyl) phosphonate; PEGDA: Polyethylene glycol diacrylate.

5.2. Design strategies for high-resolution digital light processing printing

5.2.1. Bioink criteria for high-fidelity digital light processing printing.

Bioink development is fundamental to the progress of DLP bioprinting. Particularly, the biocompatibility and functional performance of the bioink must be prioritized during early-stage formulation. Hydrogel-based bioinks are especially suitable for this purpose owing to their inherent biological compatibility and supportive interactions with cells. Therefore, bioinks must be photocurable bioactive materials that combine suitable physicochemical properties with strong biocompatibility to support accurate layer-by-layer polymerization while maintaining their intended biological function.[61]

An ideal photocurable bioink must satisfy several performance requirements to achieve high-fidelity printing. The bioink should exhibit sufficient fluidity to ensure rapid, uncured flow into the gaps between layers, enabling efficient recoating and preventing structural defects. Additionally, a high photo-crosslinking rate is essential during the initial curing step to solidify each layer within seconds and minimize printing time. Finally, a high cross-linking density must be maintained to achieve adequate stiffness and structural stability (Figure 1e). For example, PEGDA-based bioinks are widely recognized for their favorable printing characteristics—particularly their high fluidity, rapid photo-crosslinking rate, and ability to achieve a dense crosslinked network. Thus, PEGDA acts as an efficient photocurable matrix for DLP bioprinting. Yu *et al.*[58] have shown that PEGDA exhibits both faster crosslinking and a higher crosslinking density than gelatin methacryloyl (GelMA) under DLP conditions, resulting in improved printing fidelity and more reliable structural formation. In addition to the choice of the base biomaterial, the concentration of PIs plays a critical role in determining DLP printability. Tong *et al.*[62] have reported that an increase in LAP concentration significantly accelerated the photo-crosslinking rate of silk fibroin methacrylate (SilMA) bioinks. Higher LAP levels reduce curing time and enhance polymerization efficiency, thereby improving layer formation during printing. Nevertheless, the use of higher PI concentrations requires careful consideration of biocompatibility, as excessive LAP may cause cytotoxicity. Therefore, optimizing LAP levels is essential to achieve rapid curing performance balanced with cell viability and overall biological safety. Another important consideration in bioink design is the incorporation of PAs such as tartrazine, Orange G, and Maxgard® R1800. PAs function by competitively absorbing incident light and dissipating the energy as heat. This helps reduce light scattering in the X–Y plane and control curing depth along the Z axis.[63,64] By lowering the intensity of scattered light below the polymerization threshold, PAs suppress unintended crosslinking outside the projected pattern, enabling the fabrication of fine features such as hollow channels and microscale pores (Figure 2b and 2c). For example, Huh *et al.*[64] have shown that the inclusion of PAs significantly improved printing fidelity by reducing light scattering and enhancing spatial resolution during photopolymerization. Figure 2b shows the impact of PAs on printability. Bioinks without PAs exhibited pronounced over-curing; however, the incorporation of PAs effectively suppressed this over-curing behavior. Furthermore, PAs lowered the intensity of scattered light below the polymerization threshold, thereby suppressing unintended crosslinking outside the projected pattern, enabling the fabrication of fine features, such as hollow channels and microscale pores, by improving curing confinement and printing precision. However, the biocompatibility of PAs must be carefully evaluated, as excessive PA concentrations can induce cytotoxicity and adversely affect cell viability. In fact, optimal performance is typically achieved at PA concentrations of 0.05–0.5%, which balance high printing resolution with adequate interlayer bonding and crosslinking density.[63]

5.2.2. Relationships between rheological behavior and printability

Optimizing the printing parameters solely through experiments is both costly and time-consuming. Therefore, the printability of a bioink must be evaluated before printing. In this context, a bioink must exhibit adequate flowability and rapid molecular diffusion for efficient photocuring, as these enhance reaction kinetics and reduce overall printing time.[58,65-68] Among the formulation parameters, viscosity is particularly critical. DLP-printable bioinks typically require viscosities in the range of 0.2–10 Pa·s to ensure smooth processing. Resins with excessively high viscosity obstruct the recoating process and reduce printing resolution, whereas those with very low viscosity (<0.2 Pa·s) fail to properly wet the resin vat, resulting in unstable and poorly controlled printing (Figure 2d).[65] Vazquez-Martel *et al.*[66] assessed the suitability of functionalized vegetable oils for DLP printing by measuring the viscosity using a rotational viscometer. They found that olive and canola oils exhibited Newtonian behavior, whereas sunflower and soybean oils exhibited pronounced shear thinning. Nevertheless, all formulations exhibited a DLP-printable viscosity range (0.2–10 Pa·s; shown in green in Figure 2e). Furthermore, they noted that molecular diffusion decreased as viscosity increased, slowing polymerization and increasing the critical curing energy (E_c). This explains the higher E_c of soybean oil ink (18.49 mJ/cm^2) compared with those of

sunflower- and canola-oil inks despite similar acrylate functionalization levels. Yu *et al.*[58] found that fluidity increased as bioink viscosity decreased, enabling rapid gap filling and preventing structural deformation during printing. Furthermore, 10% GelMA exhibited a viscosity comparable to that of commercial resins, resulting in good flowability.

The smooth separation of the cured layer from the uncured bioink is essential to ensure accurate and reliable printing during the recoating process. In fact, after each layer is cured, the uncured bioink is required to readily refill the gap to enable the formation of the subsequent layer (Figure 2f). Hence, photorheological analysis is widely performed to evaluate the photo-crosslinking behavior of bioinks to predict their curing kinetics and mechanical evolution under light exposure.[21,58,69-71] The storage modulus (G') represents the ability of the material to store elastic deformation energy, and it is indicative of its elastic stiffness; the loss modulus (G") reflects energy dissipation during viscous deformation, and it corresponds to the viscous behavior of the material. During photo-crosslinking analysis, G' and G" are continuously monitored as the bioink undergoes light-induced crosslinking. The point at which G' and G" intersect is defined as the gel point, and the time required to reach this point is referred to as the gelation time. In DLP bioprinting, high printing resolution requires the efficient separation of the cured structure from the uncured bioink. This occurs when the crosslinked construct possesses high stiffness and the uncured ink shows low viscosity. The parameter ΔG is defined as the difference in modulus between the cured and uncured states, and it reflects the rheological contrast between the solidified structure and remaining hydrogel.[58] For example, Tong *et al.*[62] found that SilMA showed improved printing fidelity at higher ΔG values than at lower ΔG values. Moreover, an increase in bioink concentration increased the difference between G' and G"′, following the initiation of photopolymerization (Figure 2h and 2i). Typically, complete crosslinking is impractical, and experimental evidence indicates that optimal crosslinking density is achieved at approximately 80% of the maximum $\log_{10}$(G'). Therefore, this level is considered the ideal exposure condition (printable window) for DLP printing (shown in gray in Figure 2g).[58,62] Similarly, Yu *et al.*[58] reported that increasing the GelMA bioink concentration increased the ΔG values, indicating a high degree of contrast between the solidified and uncrosslinked states. This behavior may be attributed to the increased probability of C=C double-bond interactions within GelMA molecules during photopolymerization, enhancing the crosslinking density and overall reaction efficiency. Thus, higher GelMA concentrations promoted faster crosslinking kinetics and improved printing-based bioprinting (PBP) performance, yielding constructs with superior structural fidelity. Additionally, they evaluated the effect of PAs and found that increasing PA concentration reduced the ΔG value, indicating a reduction in the stiffness of the printed constructs. These results highlight the importance of optimizing the PA concentration prior to printing to achieve balanced mechanical properties and printing performance.

In addition, the elastic behavior of the printed construct needs to dominate the viscous behavior for stable shape retention. A large difference between G' and G" corresponds to improved shape fidelity. This behavior is quantified by the ΔM parameter, defined as the logarithmic difference between G' and G" after full light exposure during PBP (Figure 2g). Tong *et al.*[62] showed that ΔM increases from the gel point onward, indicating progressive crosslinking and network reinforcement in SilMA under continuous illumination. Higher ΔM values correspond to increased elasticity, improving printing resolution and structural fidelity (Figure 2h and 2i).

Another important factor in the DLP printing process is the viscoelastic dynamics of bioink—particularly under the mechanical stresses induced during recoating. G' remains consistently higher than G", indicating that bioinks behave as an elastic solid across a wide range of strains. This demonstrated that the material can absorb mechanical stress without substantial deformation, while maintaining structural stability (Figure 2j and 2k). The frequency-dependent rheological behavior of the bioink also demonstrated its suitability for dynamic applications. As shown in Figure 2l, both G' and G" increased with frequency, while the phase angle decreased, indicating enhanced elastic dominance at higher frequencies. This behavior suggests improved structural stability, rapid recovery after deformation, and strong resistance to repetitive or fluctuating mechanical stresses.[71-75] Yang *et al.*[76] reported that as frequency increased, the GelMA and collagen methacrylate (ColMA) bioinks exhibited stable viscoelastic behavior with G' consistently exceeding G" across the tested range. In the linear viscoelastic region, the G' of ColMA-S was 4.67-fold higher than that of GelMA-S, indicating superior scaffold stiffness. Furthermore, frequency-dependent oscillatory shear measurements confirmed the predominantly elastic gel behavior of both scaffolds. Additionally, the strain-dependent oscillatory rheology showed that G' of 0.5% ColMA and 5% GelMA DLP-printed scaffolds remained constant within the linear viscoelastic region (LVR), confirming their viscoelastic, solid-like behavior.

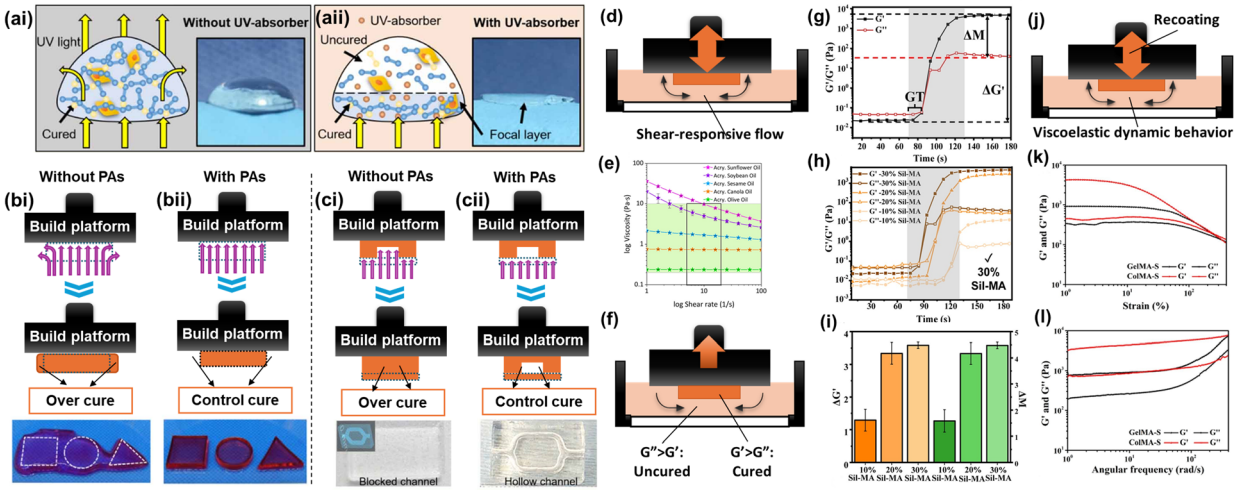

Figure 2. Key photophysical and rheological properties governing digital light processing (DLP) printability. (a) Effect of photoabsorber-mediated attenuation on light penetration depth in bioinks. Modified with permission from Huh *et al.*[64] Copyright © 2021 IOP Publishing Ltd. (b & c) Efficacy of photoabsorbers (PAs) on cure depth control. Modified with permission from Huh *et al.*[64] Copyright © 2021 IOP Publishing Ltd. (d) Schematic representation of bioink flow during printing (the arrow indicates the flow behavior of the bioink). (e) Viscosity analysis of bioink. Modified with permission from Vazquez-Martel *et al.*[66] Copyright © The authors. (f) Schematic representation of the phase-separation mechanism of cured and uncured bioink during printing (arrow sign indicated the flow behavior of bioink). (g) ΔG value and ΔM value analysis of UV-curable printing ink. Modified with permission from Tong *et al.*[62] Copyright © 2025 American Chemical Society. (h & i) Photo-rheological characterization of a UV-curable printing ink under varying exposure times. Modified with permission from Tong *et al.*[62] Copyright © 2025 American Chemical Society. (j) Schematic representation of dynamic viscoelastic behavior of bioink during printing (arrow sign indicated the flow behavior of bioink). (k) Shear strain evaluation of bioink for DLP printing. Modified with permission from Yang *et al.*[76] Copyright © 2024 Elsevier B.V. (l) Angular frequency analysis of bioink for DLP printing. Modified with permission from Yang *et al.*[76] Copyright © 2024 Elsevier B.V.

5.2.3. Jacobs' working curve and application in printability analysis

Jacobs' working curve is a fundamental analytical model in vat polymerization techniques, such as DLP, because it defines the relationship between absorbed light energy and the resulting cured thickness of a material. This model is derived from the Beer–Lambert law, which describes the exponential attenuation of light intensity as it propagates through the bioink owing to absorption by PIs and other light-absorbing components.[77-80] This relationship is mathematically expressed by the Jacobs' working curve equation:

$$C_d = D_p ln\left(\frac{E_0}{E_c}\right) \quad (1)$$

where C_d indicates the cure depth (thickness of solidified bioink); D_p indicates light penetration depth; E_0 indicates incident radiant exposure (energy per unit area); and E_c indicates critical exposure (minimum energy required to initiate gelation of bioink).

Typically, layer thickness is selected as 50–100% of the calculated cure depth, and Jacobs' working curve helps predict the suitable layer thicknesses to ensure sufficient interlayer overlap and strong bonding between successive layers. The definition of exposure energy:

$$E_0 = I_0 \times t \quad (2)$$

indicates that the total radiant dose delivered to the bioink is determined by the applied light intensity (I_0) and exposure time (t). Exposure time may be precisely controlled by rearranging the governing equation (**Equation 1**) to identify the desired cure depth without requiring excessive energy input. Bioinks with lower critical exposure require shorter exposure times, which enhance vertical resolution and mitigate over-curing-related effects such as dimensional distortion and surface fidelity loss. Overall, Jacobs' working curve provides a systematic framework for balancing cure depth, resolution, and printing speed.[78,81-84] For example, Vazquez-Martel *et al.*[66] applied the Jacobs' working curve model to predict the optimal exposure time and layer thickness for DLP printing. The cure depth was evaluated by exposing the inks to a fixed light intensity of 25 mW/cm^2 at varying exposure times and plotting the penetration depth (D_p) as a function of exposure energy using Jacobs' working curve. They analyzed six vegetable oil-based inks and found that canola-based (C_d = 103 ± 3.5 μm) and sunflower oil-based (C_d = 104 ± 3.5 μm) inks exhibited the highest curing depth (Figure 3a).

This analysis helped determine the optimal exposure time (1.15–1.20 s) and layer thickness (100 μm), based on which canola oil- and sunflower oil-based inks were used to print a plant and a helical sculpture, respectively (Figure 3b). In another study, Li *et al.*[80] developed a theoretical framework for predicting DLP printing conditions based on Jacobs' working curve. They constructed a model to evaluate both the solid- and liquid-phase absorbances and systematically evaluated solid-phase absorbance, liquid-phase absorbance, and gelation time to derive a modified predictive equation to determine the optimal printing parameters (Figure 3c).

Within this framework, the curing of the DLP printing process comprised two main phases. In the initial phase, the photocurable solution is exposed to UV light for a predefined duration known as the threshold time (t_T), resulting in a partially cured or pre-cured state. Subsequently, 3D structures were fabricated through a layer-by-layer curing process, during which the pre-cured material was further irradiated for an additional exposure time (**Δt**). This led to complete curing over a defined thickness in accordance with Jacobs' working curve. Notably, the absorbance of the photocurable material was tuned by adjusting the concentration of the photoabsorber to exert precise control over t_T and **Δt** for a given material system. Subsequently, after the recoating time (t_R) had elapsed, the next-layer printing occurred according to this mechanism until the full model was printed (Figure 3d). Additionally, the gelation time was experimentally determined using a rheometer and was incorporated into the developed predictive equation:

$$t_H = t_T \cdot \left[\frac{A_s - A_l}{A_s} + \frac{A_l}{A_s} . \exp\left(-A_s . H\right) \right] \quad (3)$$

where t_H indicates the exposure time for curing thickness H; t_T indicates threshold time; A_s indicates solid absorbance of bioink; A_l indicates liquid absorbance of bioink; and H indicates layer thickness.

They used this model to validate their theoretical predictions through experiments conducted with 20% PEGDA hydrogels. After experimentally determining the A_l, A_s, and t_T in **Equation 3**, Jacobs' working curve for PEGDA hydrogels could be theoretically predicted (black lines, L_t) and compared with the experimentally measured cured thicknesses at different exposure times (red points) and their fitted curves (red dashed lines, L_e). The intersection of L_e with the exposure-time axis is defined as t_e (experimental exposure time). Although L_t and L_e were nearly parallel, the difference between t_T and t_e, which is defined as the threshold time deviation:

$$\Delta t_T = t_T - t_e \quad (4)$$

varied with the PA concentration (C_{UV}). This deviation acted as a quantitative indicator of the accuracy of the theoretical prediction, and it increased from −0.4 s to 0.8 s as C_{UV} increased (Figure 3e). The variation Δt_T is divided into three distinct regions based on the UV-absorber concentration (Figure 3e). When C_{UV} is 0–0.15% (yellow region), Δt_T is negative, indicating that the actual critical energy required to pre-cure PEGDA hydrogels exceeds the theoretically predicted value. In contrast, when C_{UV} is >0.2% (blue region), Δt_T becomes positive, suggesting that experimental pre-curing occurs faster than that predicted by the theoretical model. Notably, when C_{UV} is in the 0.15–0.2% range (green region), Δt_T approaches zero, implying a close agreement between the theoretically predicted Jacobs' working curve and experimental data. Consequently, the UV-absorber concentration within this green region was identified as the optimal range for PEGDA hydrogels because it yielded the most accurate theoretical prediction of Jacobs' working curve. Using this plot, they determined the exposure time as 2.79 s for a 10-μm layer thickness and printed three periodic surface constructs and MNs at high resolution (Figure 3f and 3g)**.** Overall, Jacobs' working curve aids in determining the optimal exposure time and appropriate cure thickness while significantly reducing experimental effort and material waste.

5.2.4. Analysis of printing defects

Theoretical models, such as Jacobs' working curve, are widely used in DLP printing to estimate curing depth, exposure time, and layer thickness; however, they rely on ideal assumptions, such as uniform light propagation and homogeneous material properties. In practice, deviations from these assumptions result in discrepancies between theoretical predictions and experimental outcomes, leading to printing defects. These errors are defined as the differences between the fabricated construct and the intended digital design. They are inherent to DLP printing and primarily arise from light scattering and excessive curing in the depth direction. Owing to the layer-by-layer nature of vat polymerization, printing errors are systematically categorized into 2D errors that occur within individual layers and 3D errors that occur along the vertical (Z) direction between successive layers.[58,73,75,80,82,85]

Two-dimensional printing errors occur due to lateral light scattering, which causes unintended crosslinking beyond the projected exposure area and reduces in-plane (XY) resolution. The extent of this scattering is determined by material properties such as polymer concentration, molecular heterogeneity, and phase behavior. Although light scattering cannot be eliminated, its influence may be

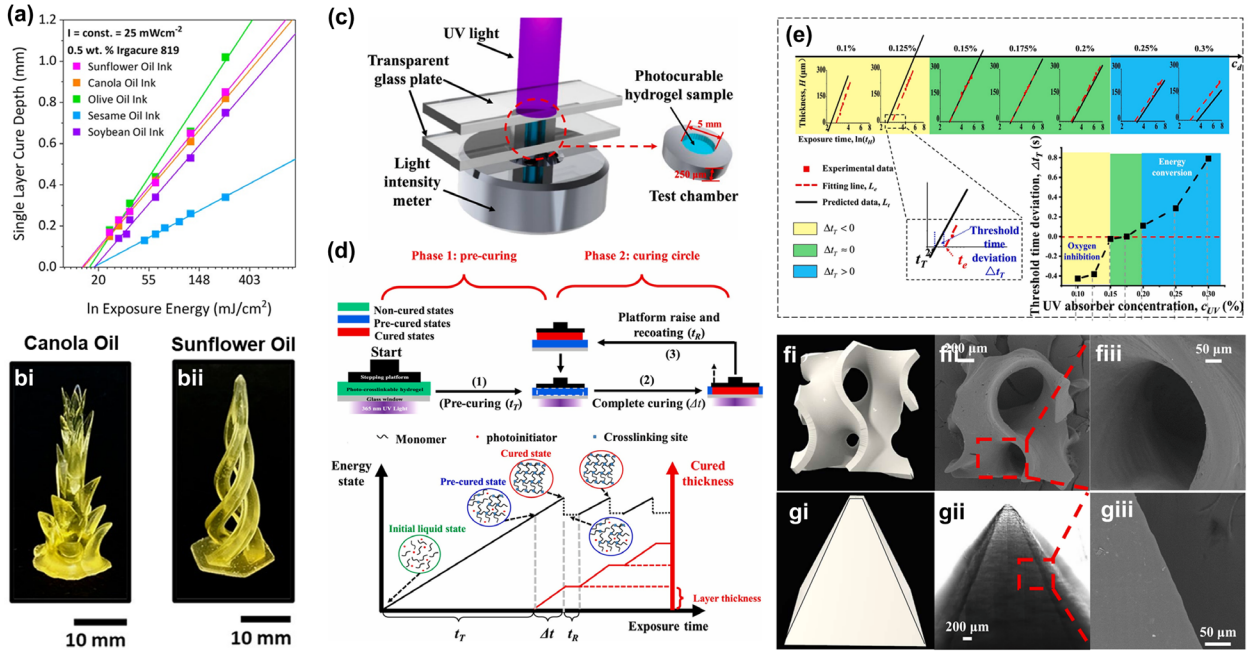

Figure 3. Influence of optical properties on photopolymerization and printing fidelity in digital light processing (DLP) bioprinting. (a) Jacobs' working curve plot for six vegetable oil bioinks. (b) Printed object of canola oil and sunflower oil bioinks (scale bar: 10 mm). (c) Designed model for the collection of bioink absorbance. (d) Schematic representation of the mechanism of photopolymerization during DLP printing. (e) Jacobs' working curve plot by varying photo-absorber concentrations. (f) Helical structure printed using polyethylene glycol diacrylate (PEGDA) bioink (scale bars: [fii] 200 μm and [fiii] 50 μm). (g) Microneedle printed using PEGDA bioink (scale bars: [gii] 200 μm and [giii] 50 μm). (a–b) Modified with permission from Vazquez-Martel *et al.*[66] Copyright © The authors. (c–g) Modified with permission from Li *et al.*[80] Copyright © 2020 Elsevier B.V.

mitigated by incorporating light absorbers that attenuate scattered photons below the polymerization threshold. However, this mitigation strategy reduces the effective incident light intensity, thereby slowing polymerization kinetics and limiting crosslinking density. Consequently, theoretical predictions must be experimentally adjusted to balance lateral resolution and curing efficiency.[86-88] Yu *et al.*[58] showed that patterned light was projected onto the bottom of the resin vat and underwent lateral scattering owing to the optical inhomogeneity of the partially cured GelMA during printing, leading to unintended crosslinking beyond the designed exposure region and resulting in 2D printing errors. Optimizing PA concentration, bioink concentration, light intensity, and exposure time could be beneficial for overcoming 2D printing errors.

In contrast, 3D printing errors occur because of excessive curing depth in the vertical (Z-axis) direction. Curing depth is required to slightly exceed the nominal layer thickness to ensure sufficient interlayer bonding; however, excessive overcuring leads to surface roughness, loss of vertical resolution, and dimensional distortion. In contrast, insufficient curing results in weak interlayer adhesion and structural instability—particularly in low-solid-content hydrogel bioinks. Curing depth is highly sensitive to exposure time, light intensity, bioink concentration, and light-absorber content, underscoring the limitations of using theoretical models in isolation.[58,89,90] Yu *et al.*[58] reported that decreasing light intensity reduced the crosslinking density of GelMA, whereas a sufficiently high interlayer crosslinking density was required to ensure reliable bonding between successive layers. Furthermore, inadequate crosslinking leads to structural deformation or collapse owing to the low solid content of the hydrogel bioinks. Although increasing bioink concentration or exposure conditions may enhance crosslinking, these strategies also increase the curing depth and may reduce printing precision. Therefore, an optimal balance of PAs, bioink concentrations, light intensity, and exposure time could be beneficial for controlling the curing depth and minimizing printing errors.[91]

5.3. Optimizing printing parameters for skin patch design

Key parameters for regenerative-skin-patch fabrication include exposure time, light intensity, layer thickness, and the physicochemical compatibility (temperature, pH) of the bioink; these parameters directly influence polymerization kinetics and curing behavior of photocurable materials. Improper parameter selection leads to insufficient curing,

cell cytotoxicity, weak interlayer adhesion, or over-curing-induced dimensional inaccuracies. Therefore, parameter optimization must be systematically validated through a combination of theoretical modeling (such as Jacobs' working curve) and experimental verification to ensure reliable and reproducible printing performance.[21,72,92]

In this context, both the lateral (XY axes) and vertical (Z axis) resolutions are essential metrics for evaluating printing fidelity, as they determine the feature accuracy of individual layers and the precision of interlayer stacking, respectively.[59,67,90,93-95] For example, Choi *et al.*[73] designed a composite bioink composed of GelMA and SilMA to fabricate a full-thickness skin model. Before printing the final skin construct, they evaluated printing fidelity by performing 3D square lumen printing tests in both the XY and Z directions. They found that the lumen width and height in the XY plane increased as silk-GMA concentration increased. Notably, the width-to-height ratios were close to unity for most lumens fabricated using the 10G10S (10% GelMA and 10% SilMA) formulation, indicating high lateral printing accuracy. In contrast, well-defined lumens were not observed along the Z direction for the 20G (20% GelMA) and 17.5G2.5S (17.5% GelMA and 2.5% SilMA) formulations, suggesting compromised vertical resolution. Moreover, the lumen dimensions in the Z direction increased proportionally with pore size for both the 10G10S and 15G5S formulations, indicating comparable vertical fidelity between the two compositions. In another study, He *et al.*[75] evaluated the printing fidelity in both the XY and Z directions after selecting an appropriate printing window based on exposure time (10–30 s) and light intensity (6 mW/cm^2) for wound patch development. Their results showed that reducing per-layer thickness significantly improved printing accuracy at both the lateral (XY) and vertical (Z) resolutions. Therefore, evaluating experimentally optimized printing parameters, such as layer thickness, exposure time, and light intensity, through a systematic assessment of both the lateral (XY) and vertical (Z) resolutions, is crucial following theoretical validation.

For the fabrication of skin patches, biocompatibility is one of the most critical considerations, as the photopolymerization process relies on PIs, PAs, and light irradiation, all of which can influence cellular viability and the stability of biomolecules. Therefore, successful DLP fabrication requires careful optimization of photopolymerization parameters to achieve rapid curing and high structural fidelity while maintaining a cytocompatible microenvironment.[21,63,72] For example, Tong *et al.*[62] fabricated a DLP-printed MN patch by optimizing the concentrations of PIs and PAs. By balancing biocompatibility and rheological properties, they established optimal printing conditions using 0.3% LAP and 0.05% tartrazine, with minimal light intensity (15 mW/cm^2) and exposure time (60 s). The fabricated MN patch demonstrated higher cell viability and enhanced cell proliferation compared to the control. Similarly, Fu *et al.*[63] reported that a formulation containing 0.25% LAP and 0.05% tartrazine concentration enabled the fabrication of high-fidelity, cell-laden constructs with sustained fibroblast viability and well-organized cytoskeletal architecture using DLP printing technology. This strategy highlights the versatility of DLP for fabricating vascular architectures that promote angiogenesis during skin tissue regeneration. Moreover, several studies have identified optimized LAP (0.03–0.3% w/v) and tartrazine (0.04–0.05% w/v) concentrations as an "optimal window" for achieving rapid fabrication while maintaining cell viability above 90%, which is essential for clinical translation. DLP printing should be considered based on the light wavelength. Several DLP-based printed devices have been developed with visible blue light (405–450 nm), which is beneficial for the fabrication of cell-laden or light-sensitive biomolecule skin patches.[21]

Temperature is another important processing parameter, particularly for thermoresponsive biomaterials such as GelMA. It is crucial to optimize the temperature during the printing process.[76,96] Yang *et al.*[76] demonstrated that the influence of temperature on printability varies considerably among different bioink systems. While GelMA benefits from elevated temperatures that improve fluidity and processability, collagen-based bioinks require lower processing temperatures to preserve their native triple-helical structure and biological functionality. Excessive heating may induce collagen denaturation, leading to the loss of bioactivity and mechanical performance.

6. Advances in tissue-specific bioinks for digital light processing-based printing

Vat photopolymerization techniques, such as DLP, widely use commercial resins owing to their high printing efficiency, resolution, and capacity to fabricate complex geometries. However, these resins show drawbacks, such as cytotoxicity and limited biodegradability; hence, pure nonfunctionalized photocurable inks are being used instead. Recently, PEGDA has been commonly used due to its biocompatibility, tunable mechanical properties, and rapid photopolymerization, enabling the fabrication of hydrated hydrogel scaffolds suitable for skin tissue engineering. Additionally, other acrylate-based polymers and hybrid composite formulations have been developed on the basis of biological functionality and investigated

to optimize printability, mechanical integrity, and biological performance in biomedical applications.[60,97-101] Recent research has focused on advancements in bioinks derived from natural sources that possess biological and biochemical functions that help skin tissue regeneration. Current advancements in bioinks and their properties are summarized in Table 2.

6.1. Functionalization of biomaterials for digital light processing-based skin patch development

Bioink functionalization is essential for the use of biologically relevant materials in DLP, which requires rapid light-induced polymerization to achieve high-resolution fabrication. Chemical modifications allow natural and synthetic polymers to acquire photo-crosslinkable properties while maintaining their biological functionality.[56,102,103] For example, methacrylation is the most widely used approach to render polymers photopolymerizable.[62] This is achieved by grafting methacryloyl groups onto functional side chains of natural biomaterials. For example, lysine residues are grafted onto gelatin to form GelMA, or hydroxyl groups onto hyaluronic acid to form hyaluronic acid methacrylate (HAMA).[62,104] Additionally, synthetic polymers, such as PEGDA, act as standard photocurable backbones owing to their tunable mechanical properties, despite frequently requiring blending with natural polymers to introduce cell-adhesive motifs.[56] Controlling the degree of substitution achieves sufficient crosslinking density while preserving the biological function. For example, ColMA synthesized under alkaline conditions (approximately pH 9) exhibited a high degree of substitution (approximately 68%) while maintaining its native triple-helical structure, which is essential for its mechanical stability, ECM-like activity, and bioactivity.[105] The mechanical properties of the bioink for skin patch fabrication are crucial.[106] Tong *et al.*[62] developed a silk-based bioink by optimizing methacrylation of silk fibroin using glycidyl methacrylate. This strategy enhanced the mechanical properties of Silk-based bioink and enabled high-fidelity DLP printing. In addition, dECM is characterized as an emerging biomaterial in the regenerative field, as it has the ability to closely mimic the native tissue microenvironment. Derived from natural tissues, dECM retains essential structural proteins, such as collagen, elastin, and glycosaminoglycans, as well as inherent bioactive cues that regulate cell behavior. This biomimetic composition promotes cell adhesion, proliferation, and differentiation, while also supporting angiogenesis and tissue remodeling.[107,108] Hewawasam *et al.*[109] developed functionalized dECM via thiolation-based functionalization to impart photo-crosslinkable properties. In this strategy, dECM participates in thiol–ene Michael addition reactions after the primary amines are converted into thiol groups using Traut's reagent. This enables its integration into hybrid hydrogel networks, highlighting the development of microarchitecture via DLP. Typically, these systems use polyethylene glycol (PEG)-based methacrylate backbones and undergo a two-stage crosslinking process: an initial Michael addition to form a soft tissue-mimetic hydrogel, followed by secondary photopolymerization to increase stiffness. The high molecular weight of thiolated dECM reduces the number of elastically inactive chain segments, improving network integrity and mechanical performance. Rapid gelation and faster fabrication processes can significantly enhance the clinical acceptability of fabricated patches, thereby enabling the fabrication of light-sensitive therapeutic and cell-laden scaffolds.[110] For example, Zhu *et al.*[111] developed a phenol-mediated functionalization strategy that utilizes endogenous tyrosine residues present in proteins such as collagen and casein. Under visible light irradiation, these tyrosine residues form stable dityrosine bonds in the presence of ruthenium-based photoredox catalysts, eliminating the need for extensive chemical modification. This approach is particularly effective for developing bio-adhesive and hemostatic sealants, as covalent bonding occurs both within the hydrogel network and at the tissue interface, resulting in enhanced mechanical stability and tissue adhesion. Such systems exhibit rapid gelation and strong adhesion under physiological conditions and are ideal for supporting applications in wound sealing and tissue repair while simultaneously promoting regenerative responses, such as angiogenesis and immune modulation.[102,103,111,112]

6.2. Hybrid and composite biomaterial composition for digital light processing-based skin patch development

Hybrid and composite biomaterial compositions are advantageous for integrating complementary mechanical, biological, and physicochemical properties, enabling precise optimization of printability, structural integrity, and bioactivity to suitably match the functional requirements of target tissues.[113,114] Mechanical strength is a key requirement for hybrid and composite bioinks. In DLP, this property is commonly enhanced by incorporating mechanically robust reinforcements into the bioactive hydrogel matrices, thereby enabling the fabrication of MN patches and vascular skin models with high resolution.[103] For example, Li *et al.*[115] developed a patch in which bacterial nanocellulose (BNC) was incorporated into GelMA bioinks to create a denser polymer network, increasing the compressive modulus from 16.4 kPa to 73.0 kPa and providing the necessary stiffness to support confluent cell

monolayers. Similarly, Choi *et al.*[73] developed a silk fibroin bioink used as a mechanical dopant owing to its high β-sheet folding content. This conferred superior tensile strength and resilience to silk fibroin-based hydrogels, enabling them to withstand the dynamic mechanical stresses associated with tissues such as skin, cartilage, and bone.

For better wound healing, swelling and water uptake properties are most necessary. It facilitates high cellular infiltration and nutrient support, leading to faster tissue regeneration.[116,117] For example, Zhang *et al.*[118] developed an MN patch for extracting interstitial skin fluid with an optimized HAMA-to-GelMA ratio of 8:2, achieving swelling rates that exceeded 1,200%. This facilitated rapid biomarker recovery. In another study, the incorporation of dECM into synthetic networks increased the average molecular weight between crosslinks. This modification increased the mesh size, improving nutrient diffusion and the equilibrium swelling ratio due to strong hydrogen bonding between water molecules and protein fragments, thereby facilitating wound-healing applications.[109,118] In addition, the swelling behavior and degradability of skin patches are critical factors, as they directly influence the release profile of therapeutic agents. The drug-delivery timeline should be carefully selected based on tissue condition. For example, rapid therapeutic delivery is essential for antimicrobial agents, as it enables effective elimination of pathogens in damaged skin and facilitates faster immunomodulation. In contrast, therapies involving antioxidants and angiogenic factors require sustained and controlled release to support prolonged tissue regeneration. Therefore, the design of composite materials enables the tuning of both rapid and sustained release profiles, allowing them to be matched to specific clinical timelines. HAMA-based structures are typically chosen for short-term drug delivery because they degrade in ≤1 week. In contrast, silk-based constructs provide sustained structural support lasting for a few weeks.[56,119]

The adhesive properties of patches are critical for ensuring stable and intimate bonding with the surrounding skin in wound beds. This is often achieved through biomimetic designs inspired by mollusks that use catechol-rich moieties or polyphenols such as tannic acid.[103,120,121] For example, Lu *et al.*[122] reported that dopamine-functionalized PEGDA hydrogels formed robust wet-tissue adhesion, facilitating the patch's attachment during bending and curvature conditions. In another study, Silva *et al.*[104] reported that surface functionalization with gallic acid improved adhesive strength by over 100%, an effect further amplified by the addition of Fe^{3+} ions, which facilitate coordination-based bonding. Moreover, applications involving self-healing and tissue mimicking have advanced through the bioprinting of heterogeneous models that replicate the stratified architecture of natural organs.[123,124] For example, Li *et al.*[115] designed a heterogeneous skin model incorporating a "dermal bioink" (10% GelMA/0.3% BNC) with large pores for fibroblast migration and a "basal bioink" (10% GelMA/1.5% BNC) with a dense network to support epidermal stratification. These scaffolds provide biochemical cues (growth factors and cytokines) found in native dECM, guiding lineage-specific cellular maturation. In another study, self-healing hydrogel scaffolds, known as biomimetic hydrogel bioadhesives (PTLA) system designed by Wu *et al.*,[103] comprise modified natural tanic acid (MTA), hyperbranched polylysine, and acrylic acid, and use dynamic physical interactions, such as hydrogen bonding and ionic attraction, to restore their integrity. These materials achieve rapid in situ healing, enabling the construct to recover its original stretchability and modulus after mechanical failure.

7. Digital light processing printing transdermal patches for skin tissue regeneration

Wounds caused by trauma, surgery, and burns present significant clinical challenges that require timely intervention to promote healing, prevent infection, and minimize scarring. Skin regeneration proceeds through four overlapping phases—hemostasis, inflammation, proliferation, and remodeling—each requiring distinct cellular, molecular, and microenvironmental cues.[125,126] However, wound characteristics vary considerably among patients due to differences in wound type, anatomical location, and underlying health conditions. Consequently, conventional wound dressings often fail to provide the dynamic and stage-specific support necessary for optimal tissue repair. These limitations have driven the development of advanced regenerative skin patches capable of delivering tailored structural, mechanical, and biological functions according to the evolving needs of the wound microenvironment. In this regard, DLP bioprinting offers a promising platform for fabricating patient-specific skin patches with customized architectures and therapeutic functionalities.[127,128] Recent DLP-based skin regeneration strategies and their corresponding applications are summarized in Table 3.

7.1. Antimicrobial and anti-infective skin patches

Infected wounds represent a major barrier to successful skin regeneration because bacterial colonization, biofilm formation, and toxin secretion can prolong inflammation, delay re-epithelialization, and increase the risk of systemic infection. Therefore, regenerative skin patches

should not only provide a protective physical barrier and maintain a moist wound environment but also possess active antimicrobial and anti-biofilm capabilities. Several DLP-fabricated skin patches have demonstrated effective infection control through different mechanisms.[129,130] For example, Park *et al.*[131] developed a DLP-fabricated patch for treating acne vulgaris using a dual-phase therapeutic strategy. In the initial phase, self-locking MN arrays deliver antibacterial agents, such as salicylic acid and *Cannabis sativa* extract, to disrupt *Cutibacterium acnes* biofilms and regulate excess sebum production. In the following maintenance phase, MNs loaded with anti-inflammatory and antioxidant compounds, such as chamomile, glutathione, and niacinamide, suppress inflammation and promote lesion resolution. Therapeutic evaluation indicated a rapid clinical response with an 81.4% decrease in acne lesions in ≤3 days and a pronounced decrease in sebum secretion. In another study, Chen *et al.*[132] reported a piezocatalytic bioink composed of SilMA, PEGDA, and Ag@$BaTiO_3$ (BT) nanoparticles. Under ultrasonic stimulation, the piezoelectric BT nanoparticles generate piezoelectric polarization, leading to ROS formation and strong antibacterial activity, achieving a 99.96% reduction against *Staphylococcus aureus*. This effective bacterial elimination creates a favorable microenvironment for skin tissue repair, leading to complete wound closure within 12 days. Beyond killing bacteria, clearing the bacterial-secreted cytotoxic proteins (pore-forming toxins) is essential to protect host cells from membrane damage and secondary poisoning. For example, Tao *et al.* 133 developed a bioink that combines GelMA with self-assembled polydiacetylene (PDA) nanoparticles engineered to function as toxin "decoys." These PDA nanoparticles mimic the structural and chemical features of cellular membranes, enabling them to selectively bind pore-forming toxins produced by bacteria. By capturing and neutralizing these toxins before they interact with host cells, the nanoparticles effectively prevent toxin-induced membrane damage, thereby protecting surrounding tissues and supporting skin regeneration. This system achieved nearly 100% neutralization of toxins *in vitro*. Moreover, phototherapy has also been widely applied to suppress bacterial growth while providing additional biological functionalities. Liu *et al.*[129] developed a therapeutic patch incorporating near-infrared (NIR)-assisted phototherapy, which induces ROS generation upon irradiation (Figure 4a). This process facilitates the release of MXene from the MN patch, conferring additional anti-inflammatory and antioxidant effects that accelerate wound healing. Notably, by day 7, the NIR-triggered patch group exhibited significant antibacterial efficacy, achieving 68% reductions in bacterial viability (*S. aureus*: 32.59%; *Escherichia coli*: 48.17%) under NIR irradiation compared to the control group (Figure 4d).

7.2. Immunomodulatory skin regeneration

The management of chronic wounds, particularly diabetic ulcers, represents a significant clinical challenge due to a persistent hyperglycemic microenvironment that traps the wound in a state of prolonged inflammation and high oxidative stress.[63,103,134] The primary goal of immunotherapeutic scaffolds in skin regeneration is the precise modulation of the local immune microenvironment through the regulation of macrophage polarization from the pro-inflammatory M1 state to the pro-regenerative M2 state. The prolonged dominance of M1 macrophages is a hallmark of chronic wounds and inflammatory skin disorders, in which sustained ROS and pro-inflammatory cytokine secretion impair tissue repair.[135-138] To address this, Fu *et al.*[63] developed a high-resolution DLP bioprinting platform capable of fabricating cell-laden collagen constructs that conform precisely to diabetic wound beds, ensuring intimate contact for efficient therapeutic delivery. The bioink was based on ColMA integrated with dihydromyricetin (DHM), a flavonoid with potent anti-inflammatory and antioxidant properties, and further enhanced using a multi-crosslinking strategy to improve mechanical stability in dynamic wound environments. The resulting ColMA–DHM hydrogel demonstrated effective ROS scavenging and successfully promoted macrophage polarization from M1 to M2. *In vivo* studies revealed a significant reduction in inducible nitric oxide synthase $(iNOS)^+$ (M1) cells and an increase in $CD163^+$ (M2) cells, leading to enhanced re-epithelialization and collagen deposition in full-thickness diabetic wounds. Concurrently, this immunoregulatory shift suppresses the expression of key inflammatory mediators, such as interleukin-6 (IL-6), IL-1β, and tumor necrosis factor-α (TNF-α), whose levels are typically elevated in chronic and non-healing wounds.[63,112,139] Collectively, this macrophage reprogramming strategy mitigates inflammatory tissue damage and promotes a timely transition from the inflammatory phase to the proliferative and remodeling phases of wound healing, thereby enhancing overall regenerative outcomes.

7.3. Vascularization-promoting skin patches

Vascularization is a fundamental requirement for successful skin regeneration, as newly formed tissue depends on a functional blood vessel network to sustain cellular survival and tissue remodeling. Following injury, disruption of the native vasculature creates a hypoxic and nutrient-deficient microenvironment that impairs cellular function and delays wound healing. Therefore,

a patch that promotes angiogenesis from pre-existing vasculature is crucial for faster skin regeneration.[140,141] Precise positioning and self-organization of vascular cells are key strategies in vascular tissue engineering, where co-printing heterogeneous cell populations is used to guide natural vessel formation.[141] For example, Zhou *et al.*[142] developed a biomimetic functional living skin using a GelMA/LAP/HA-NB (hyaluronic acid-N-(2-aminoethyl)-4-(4-(hydroxymethyl)-2-methoxy-5-nitrosophenoxy)-butanamide) bioink that closely replicates the native ECM. The construct featured a dense epidermis-like upper layer and a porous dermis-like lower layer containing interconnected microchannels (~200 μm) and cantilever beam structures, thereby enhancing nutrient transport and reducing flow resistance. By precisely positioning human umbilical vein endothelial cells and human skin fibroblasts, the system supported spontaneous self-organization into stable microvascular networks that persisted for over 30 days, while *in vivo* studies further confirmed enhanced neovascularization and the formation of skin appendages. Similarly, Mazari-Arrighi *et al.*[143] utilized DLP bioprinting to encapsulate endothelial progenitor cells (EPCs) within a multi-component GelMA bioink, enabling them to guide cellular organization into predefined vascular geometries. Within days, EPCs proliferated and self-assembled into branched tubular networks (10–100 μm in diameter) with lumen-like structures and tight cellular junctions, demonstrating functional connectivity through successful dye perfusion. In another approach, Choi *et al.*[73] employed a print–pause–print strategy to fabricate a full-thickness stratified skin model using SilMA and gelatin. This method allowed sequential deposition of a pre-vascularized dermal layer, additional stromal support layers, and an epidermal layer, while maintaining high cell viability (>95%). The resulting constructs exhibited enhanced CD31 expression, confirming vascular differentiation and providing adequate support for the development of upper skin layers. Collectively, these studies highlight how the integration of biomimetic architecture, precise cell positioning, and advanced fabrication strategies enables the formation of functional vascular networks in promoting effective skin tissue regeneration.

7.4. Controlled and stimuli-responsive drug delivery system for skin regeneration

A transformative approach in advanced wound care and skin regeneration is the fabrication of smart, stimuli-responsive, and controlled drug delivery systems that surpass conventional passive diffusion to achieve precisely regulated on-demand therapeutic release tailored to the dynamic physiology of the wound microenvironment.[144] The high spatial precision and layer-by-layer fabrication capabilities of DLP bioprinting enable the strategic incorporation of bioactive components (e.g., growth factors and proteins) into hydrogel matrices with a defined spatial distribution, thereby enabling localized responsiveness to specific internal or external cues.[73,122,145] For example, Li *et al.*[146] fabricated hydrogel MN patches using DLP bioprinting and loaded them with platelet-rich protein (PRP). On activation, the controlled release of PRP—a cascade of growth factors including TGF-β (transforming growth factor-beta), PDGF, FGF, hepatocyte growth factor (HGF), and VEGF—regulates cell proliferation and migration. *In vivo*, these hydrogel MN patches significantly accelerated wound healing, as evidenced by enhanced re-epithelialization and collagen deposition on day 14.

In contrast, heparin conjugation is a stimulus-responsive wound-healing strategy. Owing to its high density of negative charges, heparin functions as a molecular sequestration reservoir that selectively binds to and retains positively charged endogenous growth factors from the wound microenvironment.[147-150] This activates intrinsic healing processes without requiring exogenous growth factor supplementation. For example, Joshi *et al.*[148] developed personalized micropyramid wound dressings designed to sequester growth factors via heparin incorporation to regulate tissue regeneration. *In vivo* evaluation validated the efficacy of these dressings, as evidenced by significant improvements in wound-healing outcomes by day 14. In another study, Sun *et al.*[151] developed a succulent-inspired MN patch with controllable long-term drug release by integrating thiolated heparin, which promotes sustained growth factor sequestration and release, and graphene oxide (GO) nanosheets, which promote on-demand drug release under NIR laser irradiation. These MN patches exhibited good biocompatibility and effectively promoted endothelial cell proliferation, migration, and angiogenesis; additionally, these effects were validated *in vivo*.

Furthermore, the integration of functional nanomaterials into DLP-printed constructs has substantially enhanced the efficacy of controlled therapeutic delivery and accelerated skin tissue regeneration.[152] Nanomaterials, such as MXene, graphene oxide, and metal–organic frameworks, impart stimuli-responsiveness, enabling temperature-, pH-, or light-triggered release of bioactive agents. Simultaneously, they provide antibacterial activity, antioxidant effects, or pro-angiogenic activity.[129,149,153] For example, Yang *et al.*[154] developed a glucose-responsive MN system for diabetic and metabolically active wounds. This system uses glucose oxidase (GOx) to enzymatically convert excess glucose into hydrogen peroxide and gluconic acid. This induced localized acidification, triggering hydrogel degradation and facilitating the controlled release of therapeutics

encapsulated in carriers such as metal–organic frameworks. The GOx/MoS_2 MN platform has demonstrated high antibacterial efficacy, achieving an *in vitro* inhibition zone of 91.1%. Furthermore, both accelerated wound healing and antibacterial performance were confirmed *in vivo*, with MN-treated wounds exhibiting a 19% higher healing rate than untreated controls after seven days. Liu *et al.*[129] developed an NIR-responsive, personalized MN patch for diabetic wound management. This MXene-based eutectogel MN system (MF-MXene@MN) integrates photothermal responsiveness, antioxidant activity, and temperature-triggered drug release to enable efficient photothermal conversion and ROS scavenging (Figure 4a and 4b). A gradient-height design inspired by crocodile teeth has shown potential in enhancing tissue adhesion; additionally, DLP 3D printing enabled the fabrication of patient-specific wound dressings with resolutions of <50 μm. *In vitro* and *in vivo* evaluations showed a 94.88% wound closure rate within 10 days (Figure 4c), a 3.2-fold increase in angiogenesis, and a 68% reduction in bacterial viability (*S. aureus*: 32.59%; *E. coli*: 48.17%) under NIR irradiation compared to the control group. Also, pH- and temperature-responsive mangiferin release (88.3% cumulative release) was achieved by over five NIR cycles. These multifunctional properties synergistically accelerated wound healing, enhanced antibacterial activity, and controlled therapeutic delivery, surpassing the performance of conventional wound dressings and standard MN systems. Furthermore, controlled therapeutic delivery is essential for effective wound healing. Lu *et al.*[122] developed a curcumin-loaded micellar system (C-PNPD) that enabled sustained release (~80% over 4–5 days), ensuring prolonged therapeutic activity in infection-associated diabetic wounds. The incorporation of PF-127 micelles within a poly(N-isopropylacrylamide) (PNIPAm)-based, thermo-responsive matrix further facilitated on-demand drug release and tissue contraction, thereby enhancing treatment efficacy compared to conventional wound dressings (Figure 4e–g). *In vivo* studies demonstrated that the C-PNPD group achieved the highest wound-healing efficacy within 14 days (Figure 4h), highlighting the advantage of controlled and sustained drug delivery. Similarly, Li *et al.*[146] developed patient-specific GelMA–SilMA MN patches designed for localized delivery of PRP to accelerate wound healing. They integrated high-resolution 3D scanning and DLP-based printing with fabricated customized MN patches that precisely conformed to the unique sizes, shapes, and depths of individual wounds. These GelMA–SilMA patches exhibited appropriate mechanical strength, puncture resistance, and sustained release of growth factors, ensuring both structural stability and therapeutic efficacy. *In vivo*, these patient-specific patches were formed within seconds to minutes per layer. This ability highlights the potential of DLP for personalized regenerative medicine applications.[71,154,155]

In addition to chemical delivery, DLP-fabricated MN arrays function as mechanical stimulators that bypass the stratum corneum or epidermal layer and modulate skin regeneration through physical cues. Epidermal penetration activates peripheral sensory neurons and associated mechano-transduction pathways, leading to the upregulation of repair-related markers, such as Ki67 and cytokeratin (CK)14, and enhancing keratinocyte proliferation. Simultaneously, surface micro- and nano-topography plays decisive roles in regulating cellular behaviors, such as adhesion and migration, which are essential for tissue regeneration.[62,156] Joshi *et al.*[148] reported that micropyramidal surface architectures significantly promote cell migration compared to flat wound patches. Particularly, cells showed upward movement along the pyramidal features within 12 h of seeding, and they reached the apex by 48 h. Furthermore, quantitative analysis confirmed the time-dependent increases in migration distance. Collectively, these findings indicate that mechanically and topographically engineered wound dressing architectures actively regulate cellular responses and accelerate wound healing through physical stimulation.

7.5. Bioinspired smart transdermal patches for skin regeneration

Biological systems exhibit highly optimized structural and functional features that support mechanical robustness, adhesion, and efficient mass transport. Currently, biomimetic design strategies inspired by these natural architectures are widely adopted for developing transdermal patches in the field of skin regeneration.[4,157,158] For example, Ma *et al.*[159] developed an octopus-inspired skin–electronic interface to enhance skin adhesion for theranostic applications. They used DLP-based bioprinting to fabricate a multifunctional patch, PAMS, that integrates both diagnostic and therapeutic functions (Figure 5a and 5b). This bioinspired design exhibited moderate swelling behavior, notable mechanical deformability (up to 460% strain), high sensing sensitivity (gauge factor = 4.73), and robust controllable bioadhesion with a 109.29% increase in shear strength. Additionally, the patch exhibited reliable performance under extreme conditions, such as resistance to freezing at −20 °C. Functionally, the skin–electronic interface enabled sensitive monitoring of physiological signals, including temperature, motion, and electrocardiogram activity. In a rat frostbite model, the patch was effective in accelerating wound healing when applied as a wound dressing (Figure 5c). Collectively, this study has

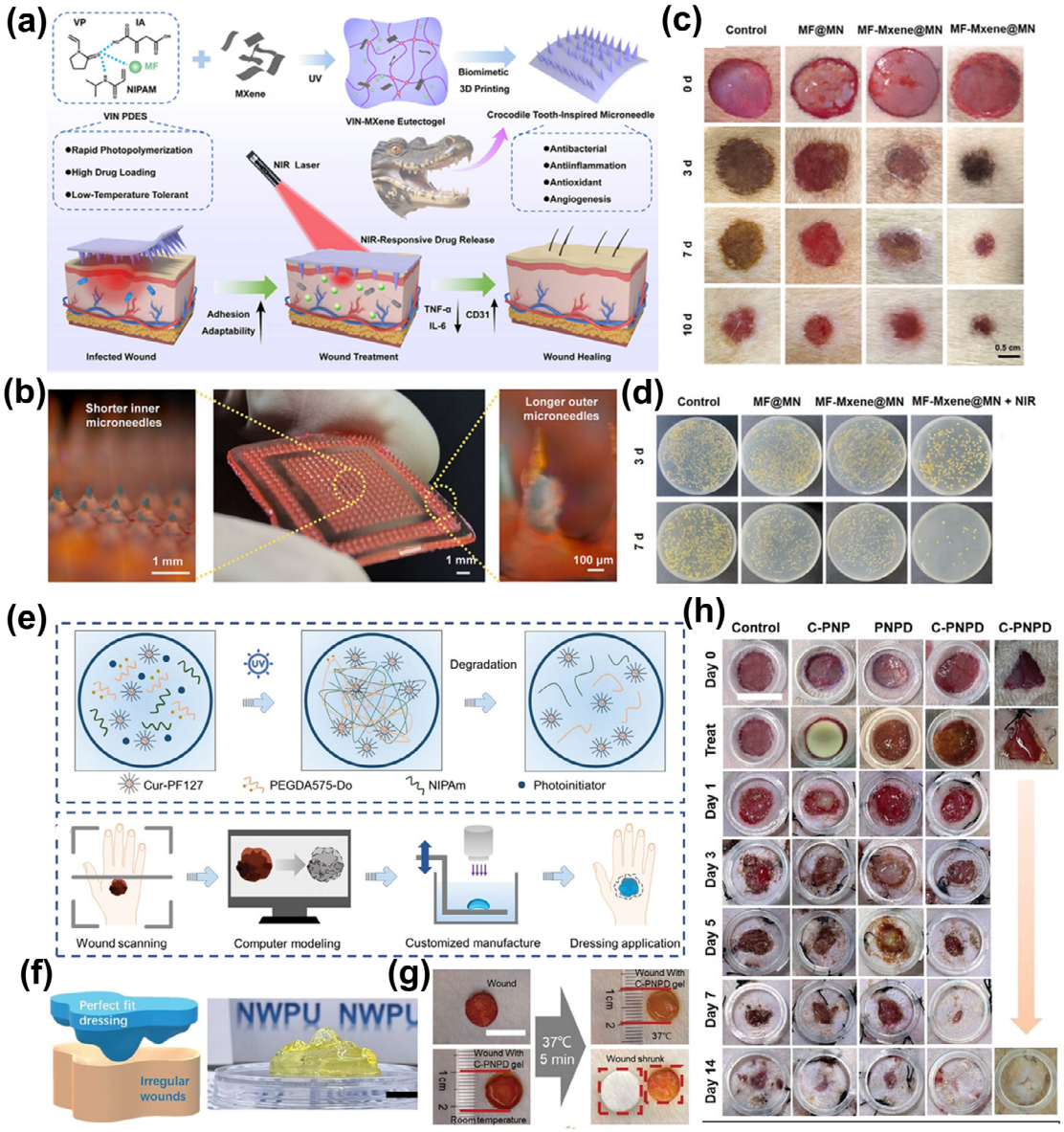

Figure 4. Digital light processing (DLP)-bioprinted smart wound healing patches. (a) Schematic representation of near-infrared (NIR)-responsive bioinspired microneedle (MN) patches fabrication and application. (b) Fabricated MN patches with shorter and longer MNs (scale bars: left to right, 1 mm, 1 mm, and 100 μm, respectively). (c) *In vivo* digital images and outlines of the wound closure rate of MN patches (scale bar: 0.5 cm). (d) *In vitro* digital image of the antimicrobial efficacy of MN patches. (e) Schematic representation of personalized adhesive patch fabrication strategies for wound healing. (f) Patch model and printed patch with a curcumin-loaded micellar system (C-PNPD) bioink (scale bar: 1 cm). (g) Temperature-responsive contractility efficacy of C-PNPD bioink (scale bar: 1 cm). (h) *In vivo* schematic diagram of wound closure rate of C-PNPD patches (scale bar: 1 cm). (a–d) Modified with permission from Liu *et al.*[129] Copyright © 2025 Wiley-VCH GmbH. (e–h) Modified with permission from Lu *et al.*[122] Copyright © 2023 Wiley-VCH GmbH.

highlighted the potential of bioinspired DLP-fabricated skin–electronic interfaces to improve adhesion, sensing performance, and therapeutic efficacy. Thus, it provides a promising strategy for next-generation bioelectronic devices, personalized diagnostics, and integrated wound care. Liu *et al.*[145] developed a coral-inspired biomimetic MN patch designed for the real-time sensing and treatment of wound infections. This design was inspired by the adaptive behavior of soft coral polyps, which extend from porous coral reefs for feeding and retract into the reef structure for protection (Figure 5d). DLP printing was performed to fabricate polycaprolactone methacrylate MNs that featured

a uniformly porous outer shell and internal cavity loaded with a heparin-based functional hydrogel incorporating therapeutic agents (e.g., minocycline) (Figure 5e). This architecture mimicked coral polyps embedded in a rigid reef, with the heparin hydrogel acting as the soft absorbent component. After penetrating the wound scab (Figure 5f), the MNs absorbed the wound exudate through surface-guiding grooves and interconnected porous networks. Exudate collection enabled real-time infection sensing through a pH-responsive colorimetric reaction that used phenol red and the adsorption of inflammatory proteins by the heparin hydrogel (Figure 5i–k). Upon detection of the infection, the system autonomously triggered rapid drug release, which was facilitated by the reversible drying–wetting behavior of the hydrogel. Once the infection was controlled, exudate levels decreased, leading to a corresponding slowdown or stoppage of drug release. Thus, a closed-loop self-regulating therapeutic response was established. For fabrication, polycaprolactone (PCL) was first methacrylated and precisely structured into a mechanically robust porous architecture using DLP printing. Subsequently, a drug-loaded heparin/HAMA hydrogel was incorporated into the scaffold via vacuum-assisted infusion, yielding the composite HepMi-PCL system (Figure 5g–h). This intelligent MN platform significantly accelerated wound healing by achieving a >200% increase in healing rate. This result highlights the potential of integrating diagnostic sensing and responsive drug delivery within a single biomimetic MN system for advanced chronic wound management. Overall, this approach provides a promising strategy for advanced management of chronic and infected wounds.

7.6. Personalized customization and wound conformity

Effective contact between the wound bed and the patch is critical for efficient fluid uptake and nutrient transport. Several studies have demonstrated that personalized,

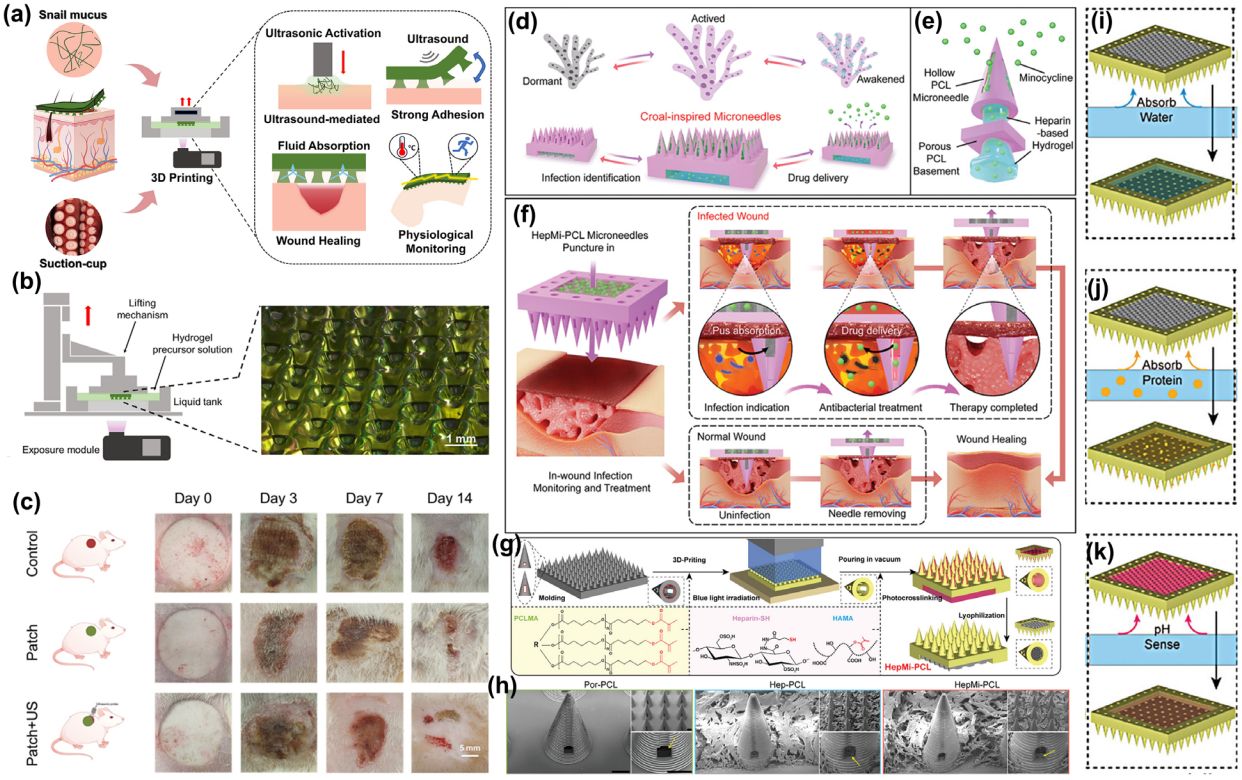

Figure 5. Digital light processing (DLP)-bioprinted multifunctional theranostic wound healing patches. (a) Schematic representation of octopus- and snail-inspired bio-adhesive suction patches and their therapeutic application process. (b) DLP-printed bioinspired suction patches (scale bar: 1 mm). (c) *In vivo* digital images of wound-healing efficacy of bioinspired suction patches (scale bar: 5 mm). (d–f) Schematic representation of coral-inspired multifunctional hollow microneedle (MN) patches and their therapeutic scheme for wound healing. (g) Fabrication strategies of coral-inspired hollow MN patches. (h) Fabricated porous polycaprolactone (Por-PCL), heparin (Hep)–PCL, and HepMi–PCL hollow MN patches. (i–k) Functional schematic diagram of hollow MN patches under water, protein, and acidic conditions. (a–c) Modified with permission from Ma *et al.*[159] Copyright © 2024 Acta Materialia Inc. (d–k) Modified with permission from Liu *et al.*[145] Copyright © 2024 Wiley-VCH GmbH.

conformal scaffolds that closely match the wound geometry significantly enhance therapeutic outcomes compared to conventional flat patches. Therefore, personalized wound patches are particularly advantageous, as they conform to the unique geometry, size, and depth of each patient's wound; they also help maintain an optimal microenvironment that supports rapid and effective healing. DLP-based bioprinting is an effective platform for fabricating customized dressings. It integrates high-resolution 3D scanning with digital CAD modeling to produce patient-specific patches that match the wound bed with notable precision—often with resolutions of <50 μm. This intimate "perfect fit" eliminates gaps where bacteria might proliferate and enhances local healing efficiency. Moreover, the rapid layer-by-layer fabrication capability of DLP enables on-demand creation of complex anatomical structures, such as asymmetric multilayer hydrogels and individualized ear grafts, and force-induced wound contraction.[45,148,160] For example, Lu *et al.*[122] addressed diabetic wound healing by developing personalized wound-conforming patches. They captured high-resolution images of the wound bed and generated corresponding digital models, followed by fabrication of the dressings directly at the point-of-care (**Figure 4e** and 4**f**). The engineered patch, C-PNPD, comprised a multifunctional composite of degradable crosslinkers, such as N-isopropylacrylamide (NIPAm), curcumin-loaded Pluronic F127 micelles (Cur-PF127), and PEGDA–dopamine (PEGDA575-Do). In this system, PEGDA575–Do provided robust tissue adhesion and controlled biodegradability, whereas Cur-PF127 imparted antibacterial functionality (Figure 4d). Furthermore, the use of PNIPAm enabled thermo-responsive contractility by undergoing a phase transition at its lower critical solution temperature (32–34 °C). Below this temperature, the hydrogel remained swollen; above it, hydrophobic interactions caused water expulsion and network shrinkage, generating a contraction force. In combination with strong tissue adhesion, these MN patches significantly enhanced wound healing by promoting rapid re-epithelialization, collagen deposition, and overall tissue regeneration in ≤14 days.

Table 2. Advancements in bioinks for DLP-printed transdermal patch fabrication

Bioink types	Bioink composition	Additives & wavelength	Advancements	Advantages	References
Photo-functionalized bioink composite	Casein-based bioink (milk protein)	Ru-SPS, 450 nm	Exploiting intrinsic tyrosine residues to induce stable di-tyrosine bond formation via white-light–mediated photochemical activation using ruthenium-based catalysts.	Ultrafast gelation (2–10 s); provides robust covalent adhesion that can withstand pressures exceeding 180 mmHg without peeling force from tissue.	[111]
	dECM (decellularized ECM)-based bioink	Ru-SPS, 450 nm	The di-tyrosine bonds are formed through the coupling of tyrosyl free radicals, thereby facilitating the preservation of native bioactivity for regenerative medicine applications.	This strategy effectively mimics tissue-specific microenvironments and provides biochemical cues for lineage-specific differentiation, while Ru–SPS PI systems further reduce cytotoxicity.	[161]
	ColMA	LAP, 405 nm	Low-temperature DLP fabrication under acidic conditions (pH 3) enables a high degree of substitution (up to 98%) while preserving the triple-helical protein structure.	Maintains structural integrity with enhanced mechanical properties and resistance to enzymatic degradation compared to GelMA alone.	[76]

(*cont'd...*)

Table 2. (*Continued*)

Bioink types	Bioink composition	Additives & wavelength	Advancements	Advantages	References
	SilMA	LAP & tartrazine, 405 nm	Methacryloyl modification enhances the mechanical stability and photo-crosslinking capability of the biomaterial, facilitating the formation of stable porous 3D structures suitable for cell encapsulation.	The material exhibits enhanced tensile strength and flexibility, closely mimicking the elastic properties of native skin while providing a stable architecture for cell growth.	[73]
	GelMA–keratin methacrylate	LAP, 405 nm	Integrating GelMA & keratin methacrylate improves structural integrity and photo-crosslinking capability, enabling the fabrication of thin, high-precision patch constructs.	Enhanced crosslinking density increases bioactive binding sites, promoting cell adhesion and proliferation through cysteine-rich fragments.	[162]
	HAMA/GelMA	Tartrazine & LAP, 405 nm	Fine-tuning the bioink composition (HAMA–GelMA = 8:2 ratio) enables uniform microneedle geometry with swelling behavior exceeding 1,200%.	HAMA/GelMA composite exhibits high water retention and mechanical resilience, enabling rapid biomarker recovery while maintaining minimal invasiveness.	[118]
	Liver dECM (LdECM) methacrylate & GelMA composite	Eosin Y (EY) & TEOA, 400–700 nm	The LdECM–GelMA composite exhibits rapid crosslinking kinetics, excellent printability, and preserved native bioactivity, while demonstrating low cytotoxicity at 400–700 nm.	The hybrid composite demonstrated enhanced mechanical properties and excellent cell-friendly printability.	[163]
Multifunctional bioink composite	AMPS-Na/CMC/PEGDMA	TPO-L & LAP, 450 nm	A dual photoinitiator system (TPO-L/LAP) under 450 nm enabled fabrication through synergistic reinforcement mechanisms, including nanofiber strengthening and hydrogen/coordination bonding.	Non-UV photopolymerization minimizes cytotoxicity, while the material's high-water uptake and retention capacity significantly improve hemostatic performance.	[75]
	NIPAm, PEGDA–dopamine bioink composites (C-PNPD)	Li-TMPP & LI-LAP, 405 nm	Incorporation of thermo-responsive NIPAm enables 4D printing of dynamic constructs with temperature-triggered shape transformation, while dopamine enhances adhesiveness and PEGDA improves mechanical robustness.	Thermally induced contraction (~52% shrinkage) at physiological temperatures promotes wound closure, regulates inflammation, and maintains stable adhesive wound contact.	[122]
	NIPAm, MXene-based eutectogel (VIN–MXene–eutectogel)	TPO-L, 405 nm	Eutectogel incorporation provides bioinspired adhesiveness, while NIR-triggered MXene nanosheets exhibit efficient photothermal conversion and strong antioxidant activity.	This strategy exhibits multi-stimuli responsiveness (NIR, pH, and temperature), enhances tissue anchoring through bioinspired adhesion, and enables precise on-demand drug release.	[129]
	Zingerol-OH-based bioink	TPO, 385 nm	Zingerol modification via ether, ester, or urethane backbones enables tunable mechanical and biodegradation properties.	The zingerol-based composite exhibits intrinsic anti-biofilm and immunomodulatory activity without exogenous antibiotics.	[164]
	PTLA bioink composite (TA/HPL/AA)	TPO, 395 nm	3D printing of catechol-rich modified TA with HPL enables rapid self-healing.	The material exhibits strong wet-tissue adhesion, outperforming commercial adhesives in blood-rich environments while maintaining structural integrity at −90°C.	[103]

(*cont'd...*)

Table 2. (*Continued*)

Bioink types	Bioink composition	Additives & wavelength	Advancements	Advantages	References
	ColMA–procyanidins	LAP, 405 nm	Procyanidin incorporation enhances ColMA network stability and oxidative resistance through bio-derived crosslinking and ROS scavenging.	Procyanidins enhance mechanical properties and cell proliferation while scavenging residual free radicals generated during printing.	[105]
	GelMA & MCCA (allyl cellulose)	Tartrazine & LAP, 405 nm	The combination of GelMA with photopolymerizable allyl cellulose enhances gel fraction and degradation resistance.	Cellulose derivatives enhance the absorption and retention of wound exudates, maintaining a moist healing environment conducive to repair.	[104]

Abbreviations: AA: Acrylic acid; AMPS: 2-acrylamide-2-methyl-propanesulfonic acid; CMC: Carboxymethyl cellulose; ColMA: Collagen methacrylate; C-PNPD: Curcumin-PEGDA-NIPAM-polydopamine hydrogel composite; DLP: Digital light processing; ECM: Extracellular matrix; GelMA: Gelatin methacryloyl; HAMA: Hyaluronic acid methacryloyl; HPL: Hyperbranched polylysine; LAP: Lithium phenyl(2,4,6-trimethylbenzoyl) phosphonate; MCCA: Allyl cellulose; NIPAm: N-isopropylacrylamide; NIR: Near-infrared; PCL: Polycaprolactone; PEGDA: Polyethylene glycol diacrylate; PEGDMA: Polyethylene glycol dimethacrylate; PI: Photoinitiator; PTLA: Modified tannic acid–hyperbranched polylysine–acrylic acid hydrogel composite; ROS: Reactive oxygen species; Ru: Tris(2,2-bipyridyl) dichlororuthenium (II) hexahydrate; SilMA: Silk fibroin methacrylate; SPS: Sodium persulfate; TA: Tannic acid; TEOA: Triethanolamine; TPO: Diphenyl(2,4,6-trimethylbenzoyl)phosphine oxide; VIN: Vinyl pyrrolidone-itaconic acid-NIPAm hydrogel composite.

8. Current challenges and future outlook

Despite the significant promise of DLP bioprinting for skin regeneration, its clinical translation remains constrained by several critical challenges that necessitate targeted strategies. A primary limitation is the limited availability of photocurable bioinks that can simultaneously achieve high printability, biocompatibility, biodegradability, and long-term mechanical stability. Current systems often require trade-offs between biological functionality and structural integrity. To address this, future efforts should prioritize the development of biomimetic hybrid bioinks that integrate naturally derived polymers (e.g., GelMA, collagen, hyaluronic acid) with synthetic networks to enhance mechanical robustness while preserving bioactivity. The incorporation of dECM, dynamic or reversible crosslinking chemistries, and stimuli-responsive elements may further enable improved cell–material interactions, tunable degradation, and functional adaptability. Another major bottleneck in clinical translation is insufficient vascularization within engineered constructs, which limits nutrient diffusion and long-term tissue integration. Advanced strategies, including pre-vascularized bioinks, angiogenic factor delivery, and microfluidic-assisted vascular patterning, should be further explored to promote rapid neovascularization and functional tissue regeneration.

Manufacturing scalability and regulatory compliance also present substantial barriers. Current DLP systems are largely confined to laboratory-scale production, with unresolved issues in batch-to-batch consistency, sterilization, and storage. Notably, conventional sterilization and storage methods, such as autoclaving, gamma irradiation, refrigeration (4 °C), freezing (−20 °C/−80 °C), and lyophilization, may compromise hydrogel integrity and bioactivity, particularly in cell-laden or drug-loaded systems. To overcome these limitations, the establishment of standardized fabrication protocols, automated quality-control systems, Good Manufacturing Practice (GMP)-compliant workflows, and non-destructive sterilization techniques will be essential for ensuring reproducibility and regulatory approval.

Looking forward, several emerging technologies offer promising solutions to these challenges. Artificial intelligence and machine learning can facilitate the optimization of printing parameters, predict material performance, and enable real-time process monitoring. Hybrid manufacturing approaches that combine DLP with complementary techniques, such as electrospinning, extrusion bioprinting, and microfluidics, may further enhance mechanical performance, biological functionality, and structural complexity. Moreover, advances in patient-specific imaging, CAD, and digital manufacturing are expected to enable the fabrication of highly customized skin patches that precisely conform to irregular wound geometries and individual therapeutic requirements. The integration of biosensing platforms, wireless monitoring systems, and stimuli-responsive drug delivery mechanisms

may further transform DLP-fabricated patches into intelligent therapeutic systems capable of dynamically responding to changes in the wound microenvironment.

Table 3. DLP-printed therapeutic patches for drug delivery and skin tissue regeneration

Bioink composition	Delivered therapeutics	Therapeutic class	Molecular target	References
SilMA & PEGDA	Ag@BT (silver–barium titanate) nanoparticles	Piezocatalytic-induced antibacterial therapy & tissue regeneration	Piezocatalytic properties enable ultrasound-induced piezoelectric polarization, leading to ROS generation for the inhibition of bacterial infection.	[132]
GelMA & SilMA	Platelet-rich proteins (PRP)	Personalized microneedle (MN) patches for sustained PRP delivery to accelerate tissue regeneration	Sustained delivery of TGF-β, PDGF, FGF, HGF, and VEGF from the GSPMN patch significantly upregulates CD31 and α-SMA expression at day 7, facilitating neovascularization and enhancing the wound healing process.	[146]
ColMA & zinc ions (Zn^{2+})	Anti-wrinkle peptide (AHP-8)	AHP-8-loaded anti-aging collagenase eye patches	Upon AHP-8 release, hydroxyproline (HYP), collagen deposition, and superoxide dismutase were increased, and malondialdehyde was decreased – enhanced skin regeneration.	[165]
GelMA & PEGDA	Doxycycline, GOx, & MoS_2 (molybdenum disulfide)	Glucose-responsive antibacterial therapy & diabetic wound healing	Upon glucose stimulation, GOx catalyzes the conversion of glucose into gluconic acid and H_2O_2. The resulting gluconic acid decreases hyperglycemia and acidifies the local microenvironment, both of which are beneficial for wound healing. Simultaneously, H_2O_2 undergoes catalytic activation by MoS_2, generating bactericidal ROS that eradicate infection and support subsequent tissue regeneration.	[154]
AMPS-Na, PEGDMA, & CMC	N/A	Hemostatic & antibacterial properties for wound repair	The hemostatic and antimicrobial properties of CMC reduced blood clotting time and inhibited microbial infections caused by *Staphylococcus aureus*, *Escherichia coli*, & MRSA, thereby supporting tissue repair.	[75]
ColMA	N/A	Biomimetic personalized scaffold for skin tissue regeneration.	The unique triple-helical structure of ColMA, characterized by high proline and HYP content, significantly enhanced the expression of vimentin, α-SMA, and collagen I compared to GelMA on day 7, thereby promoting skin tissue regeneration.	[76]
SilMA & GelMA	Epidermal growth factor (EGF)	An artificial skin model for skin wound healing	The EGF-loaded skin model significantly increased the gene expression of cytokeratin 13, *FGF*, and *CD31* within two weeks, demonstrating strong potential for skin tissue regeneration.	[73]
AM & PEGDA	MXene nanosheets	Bioinspired theranostic patches with antibacterial application in wound healing	The adhesive capacity, ultrasound-mediated interfacial toughening mechanism, and antibacterial properties of MXene nanosheets collectively support wound healing within 14 days.	[159]
ColMA & DHM	HDF cells	Porous cell-laden hydrogel constructs for diabetic tissue regeneration	Prolonged antioxidant activity effectively scavenged ROS, induced macrophage phenotypic transition from pro-inflammatory M1 to pro-regenerative M2 states, and increased collagen deposition at day 18, collectively contributing to improved tissue remodeling.	[63]
GelMA & ACA	CNPs & MSCs-EVs	Auxetic, elastic, & sticky (AuxES) patches for tissue regeneration	AuxES patches upregulated *Ccr4*, *Ackr4*, *Cd7*, *Il17b*, and *Il2* gene expression, promoting the transition from an inflammatory to a proliferative microenvironment and thereby supporting wound healing.	[166]

(*cont'd...*)

Table 3. (*Continued*)

Bioink composition	Delivered therapeutics	Therapeutic class	Molecular target	References
PCLMA & heparin hydrogel	Minocycline hydrochloride (Mi)	Bioinspired porous theranostic hollow MN patches for wound infection	HepMi–PCL MN patches inhibited bacterial infection and downregulated pro-inflammatory cytokines, including TNF-α, IL-6, and IL-1β, thereby promoting tissue regeneration.	[145]
PEG-DPA, BAPO, & NVP	N/A	Bioinspired adhesive, flexible wound dressings (PD-NVP)	The antioxidant activity of PC–NVP downregulated pro-inflammatory cytokines (TNF-α, IL-6, and IL-1β) and scavenged ROS, thereby promoting wound healing by day 12.	[167]
NIPAm & PEGDA575–dopamine	Curcumin-loaded micelles	Wound-specific thermo-contractile, adhesive hydrogel scaffold (C-PNPD) for diabetic tissue regeneration	C–PNPD inhibited MRSA-induced diabetic wound infection and promoted wound healing by modulating inflammation (downregulating IL-6) and enhancing angiogenesis (upregulating VEGF).	[122]
Vinyl pyrrolidone, itaconic acid, NIPAM	Mangiferin (MF), MXene nanosheets	Bioinspired NIR-responsive MF-Mxene@MN patches for infected wound regeneration.	MF-Mxene@MNs patches inhibited *S. aureus*-associated infection, downregulated pro-inflammatory cytokines via their antioxidant potential, and supported the regeneration of infected tissue.	[129]
SG (SilMA & GelMA) & TA-Fe^{3+}	$W_{18}O_{49-x}$@Au	NIR-responsive phototherapeutic (STFWA) for wound regeneration	NIR-triggered ROS production exerted potent antibacterial effects, and protein–protein interaction analysis revealed *CDKN1A* as a central regulatory node governing cell cycle control, cellular proliferation, and immunomodulatory responses, thereby contributing to enhanced wound repair.	[168]
HAMA & PEGDA	Vascular endothelial growth factor (VEGF), graphene oxide (GO)	Bioinspired, NIR-responsive, personalized MN patches (GO/VEGF@MNs) for controlled drug release in tissue regeneration	GO/VEGF@MNs patches promoted enhanced cell proliferation, migration, and angiogenesis, as evidenced by tube formation in HUVECs *in vitro*.	[151]
SilMA, GelMA & HAMA	HaCaT cells, Cu-EGCG (copper-polyphenol)	Personalized Cu–EGCG-loaded hydrogel scaffold for infectious wound healing and scar treatment	The hydrogel scaffold exhibited potent antimicrobial and anti-inflammatory effects and enhanced angiogenesis within 10 days via activation of the HIF-1α/VEGF signaling pathway.	[112]
HEMA & PEGDA	Silver nanoparticles (AgNPs)	Antibacterial wearable hydrogel wound patch.	AgNPs disrupted bacterial protein synthesis and inhibited bacterial growth at the wound site, thereby supporting infection control and promoting tissue regeneration.	[169]
ColMA & BDDE	Retinol (VA)	Retinol-loaded personalized eye patches for antiaging therapy	Upon VA release, the HYP, collagen deposition, and superoxide dismutase were increased, and malondialdehyde was decreased—enhanced skin regeneration.	[170]
SilMA	Ferulic acid, MTX, minoxidil	MNs transdermal delivery & skin regeneration	MN treatment resulted in a higher density of positively stained cells for Ki67, CK14, TGM-1, and TGF-β compared to the control group, indicating enhanced skin microwound repair.	[62]
HA (hyaluronic acid)	Salicylic acid, niacinamide	Self-locking MN patches with antibacterial and anti-inflammatory effect for acne vulgaris	Sequential MN patches (antibacterial then anti-inflammatory) improved acne lesion repair and decreased sebum secretion by day 7.	[131]

(*cont'd...*)

Table 3. (*Continued*)

Bioink composition	Delivered therapeutics	Therapeutic class	Molecular target	References
GelMA	HDF cells & graphene	Electrical stimulation induces skin regeneration	Electrical stimulation of GelMA scaffolds seeded with HDF cells upregulated FGF2, collagen I (Col-I), and MMP9 expression, thereby promoting wound regeneration by day 7	[171]
GelMA & PEGDA	Heparin	Biomimetic sequestration of growth factors for tissue regeneration	Upon heparin release, exogenous growth factors such as VEGF are sequestered, promoting tissue regeneration by day 14.	[148]
Casein (milk protein), Ru-SPS	N/A	Adhesive, hemostatic therapy for wound repair	The hemostatic properties of tyrosine-rich proteins reduced the blood clotting index (BCI%) and thereby supported tissue repair.	[111]
HA, PVP, & dihydromyricetin	Lidocaine	MN patches drug delivery for psoriasis treatment	The DMY-LD MN patch demonstrated the ability to attenuate immune-inflammatory responses in psoriasis by inhibiting the TLR4/NF-κB signaling pathway.	[134]

Abbreviations: α-SMA: Alpha-smooth muscle actin; ACA: Acrylic acid; AM: Acrylamide; AMPS: 2-acrylamide-2-methyl-propanesulfonic acid; BAPO: Bis(2,4,6-trimethylbenzoyl)-phenylphosphine oxide; BDDE: 1,4-butanediol diglycidyl ether; C-PNPD: Curcumin-PEGDA-NIPAM-polydopamine hydrogel composite; CK14: Cytokeratin 14; CMC: Carboxymethyl cellulose; CNP: Curcumin nanoparticles; ColMA: Collagen methacrylate; DHM: Dihydromyricetin; DPA: Dopamine; EV: Extracellular vesicles; FGF: Fibroblast growth factor; GelMA: Gelatin methacryloyl; HAMA: Hyaluronic acid methacryloyl; HDF: Human dermal fibroblasts; HEMA: 2-hydroxyethyl methacrylate; HGF: Hepatocyte growth factor; HIF-1α: Hypoxia-inducible factor-1 alpha; HUVEC: Human umbilical vein endothelial cell; IL: Interleukin; MMP9: Matrix metalloproteinase-9; MRSA: Methicillin-resistant *Staphylococcus aureus*; MSC: Mesenchymal stem cells; N/A: Not available; MTX: Methotrexate; NF-κB: Nuclear factor-kappa B; NIPAm: N-isopropylacrylamide; NIR: Near-infrared; NVP: N-vinylpyrrolidone; PCLMA: Polycaprolactone methacrylate; PDGF: Platelet-derived growth factor; PEG: Poly(ethylene glycol); PEGDA: Polyethylene glycol diacrylate; PEGDMA: Polyethylene glycol dimethacrylate; PVP: Polyvinylpyrrolidone; ROS: Reactive oxygen species; Ru: Tris(2,2-bipyridyl) dichlororuthenium (II) hexahydrate; SilMA: Silk fibroin methacrylate; SPS: Sodium persulfate; STFWA: W18O49-x@Au NPs loaded SilMA-GelMA-TA-Ferric- hydrogel composite; TA: Tannic acid; TGF-β: Trasnforming growth factor beta; TGM-1: Transglutaminase 1; TLR4: Toll-like receptor 4; TNF-α: Tumor necrosis factor-alpha.

9. Conclusion

Digital light processing-based bioprinting is a powerful platform for fabricating high-resolution, customizable transdermal patches and skin-regenerative constructs with precise control over their geometry, composition, and therapeutic function. Despite challenges related to material limitations, mechanical stability, and clinical translation, advances in bioink design, nanomaterial integration, and intelligent manufacturing strategies are steadily addressing the issues that hinder DLP bioprinting in clinical applications. Overall, combining DLP bioprinting with stimuli-responsive systems, immunomodulatory therapies, and real-time sensing technologies could lead to the advent of next-generation smart patches with enhanced healing efficacy and high clinical applicability, transforming wound care from a passive treatment to an active, personalized intervention.

Acknowledgments

None.

Funding

This work was supported by a two-year research grant from Pusan National University.

Conflict of interest

The authors declare they have no competing interests.

Author contributions

Conceptualization: Fowzul Islam Fahad, Byoung Soo Kim
Writing–original draft: Fowzul Islam Fahad
Writing–review & editing: All authors

Ethics approval and consent to participate

Not applicable.

Consent for publication

Not applicable.

Availability of data

Not applicable.

References

1. Dąbrowska A, Spano F, Derler S, Adlhart C, Spencer ND, Rossi RM. The relationship between skin function,

barrier properties, and body-dependent factors. *Skin Res Technol.* 2018;24(2):165-174.

doi: 10.1111/srt.12424

2. Menon GK, Kligman AM. Barrier functions of human skin: a holistic view. *Skin Pharmacol Physiol.* 2009;22(4):178-189.

doi: 10.1159/000231523

3. Wong R, Geyer S, Weninger W, Guimberteau JC, Wong JK. The dynamic anatomy and patterning of skin. *Exp Dermatol.* 2016;25(2):92-98.

doi: 10.1111/exd.12832

4. Fahad FI, Ahn M, Kim BS. Advanced 3D-printed microneedle patches for smart drug delivery in wound care. *Int J Bioprint.* 2025;11(2):184-215.

doi: 10.36922/ijb.8514

5. Pang Y, Liu B, Jiang J, *et al*. Recent advances in immunocompetent human skin-on-chip models: Construction strategies and biomedical applications. *Bioact Mater.* 2026;64:94-134.

doi: 10.1016/j.bioactmat.2026.04.030

6. Sen CK. Human Wound and Its Burden: Updated 2020 Compendium of Estimates. *Adv Wound Care.* 2021;10(5):281-292.

doi: 10.1089/wound.2021.0026

7. Rodriguez-Rodriguez N, Martinez-Jimenez I, Garcia-Ojalvo A, *et al*. Wound Chronicity, Impaired Immunity and Infection in Diabetic Patients. *MEDICC Rev.* 2022;24(1):44-58.

doi: 10.37757/MR2021.V23.N3.8

8. Nuutila K, Eriksson E. Moist Wound Healing with Commonly Available Dressings. *Adv Wound Care.* 2021;10(12):685-698.

doi: 10.1089/wound.2020.1232

9. Farahani M, Shafiee A. Wound Healing: From Passive to Smart Dressings. *Adv Healthc Mater.* 2021;10(16):e2100477.

doi: 10.1002/adhm.202100477

10. Tiwari R, Pathak K. Local Drug Delivery Strategies towards Wound Healing. *Pharmaceutics.* 2023;15(2):634.

doi: 10.3390/pharmaceutics15020634

11. Norouzi S, Shemshaki NS, Norouzi E, *et al*. Recent advances in biomaterials for tissue-engineered constructs: Essential factors and engineering techniques. *Mater Today Chem.* 2024;37:102016.

doi: 10.1016/j.mtchem.2024.102016

12. Dutra Alves NS, Reigado GR, Santos M, *et al*. Advances in regenerative medicine-based approaches for skin regeneration and rejuvenation. *Front Bioeng Biotechnol.* 2025;13:1527854.

doi: 10.3389/fbioe.2025.1527854

13. Golebiowska AA, Intravaia JT, Sathe VM, Kumbar SG, Nukavarapu SP. Decellularized extracellular matrix biomaterials for regenerative therapies: Advances, challenges and clinical prospects. *Bioact Mater.* 2024;32:98-123.

doi: 10.1016/j.bioactmat.2023.09.017

14. Hu T, Fang J, Shen Y, *et al*. Advances of naturally derived biomedical polymers in tissue engineering. *Front Chem.* 2024;12:1469183.

doi: 10.3389/fchem.2024.1469183

15. Uchida DT, Bruschi ML. 3D Printing as a Technological Strategy for the Personalized Treatment of Wound Healing. *AAPS PharmSciTech.* 2023;24(1):41.

doi: 10.1208/s12249-023-02503-0

16. Singh S, Kumar M, Kumar D, Kumar S, Chopra S, Bhatia A. Therapeutic Precision: Unveiling the Potential of 3D Printing in Drug Delivery, Tissue Engineering, and Regenerative Medicine. *3D Print Addit Manuf.* 2025;12(5):447-473.

doi: 10.1089/3dp.2023.0364

17. Chen SS, Wang M. Fabrication, Properties, and Applications of Scaffolds for Bone Tissue Regeneration. *Adv Mater Technol.* 2026;11(9):e01877.

doi: 10.1002/admt.202501877

18. Li Y, Zhang X, Zhang X, Zhang Y, Hou D. Recent Progress of the Vat Photopolymerization Technique in Tissue Engineering: A Brief Review of Mechanisms, Methods, Materials, and Applications. *Polymers.* 2023;15(19):3940.

doi: 10.3390/polym15193940

19. Wang XH, Liu JH, Zhang Y, *et al*. Advances in precision microfabrication through digital light processing: system development, material and applications. *Virtual Phys Prototyp.* 2023;18(1):e2248101.

doi: 10.1080/17452759.2023.2248101

20. Zhu Y, Guo S, Ravichandran D, *et al*. 3D-Printed Polymeric Biomaterials for Health Applications. *Adv Healthc Mater.* 2025;14(1):e2402571.

doi: 10.1002/adhm.202402571

21. Alparslan C, Bayraktar Ş. Advances in Digital Light Processing (DLP) Bioprinting: A Review of Biomaterials and Its Applications, Innovations, Challenges, and Future Perspectives. *Polymers.* 2025;17(9):1287.

doi: 10.3390/polym17091287

22. Tsegay F. *3D Printing Hydrogel Based Smart Patches for Wounds*. Master's Thesis. Abu Dhabi, UAE: Khalifa University of Science; 2022.

23. Ye T, Chai MY, Wang ZX, Shao TR, Liu J, Shi XT. 3D-Printed Hydrogels with Engineered Nanocrystalline Domains as Functional Vascular Constructs. *ACS Nano.* 2024;18(37):25765-25777.

doi: 10.1021/acsnano.4c08359

24. Pilavci E, Altan E, Guldorum Y, *et al*. Hydrogel-Based Microneedles Via 3D DLP Printing: A New Frontier in Controlled Drug Delivery. In: *Microneedles (MNs)-Based Technology*. Singapore: Springer; 2025:87-116.

doi: 10.1007/978-981-96-3916-8_4

25. Zhang W, Hu J, Wu H, Lin XF, Cai LM. Stimuli-responsive hydrogel dressing for wound healing. *APL Mater.* 2025;13(1):010601.

doi: 10.1063/5.0245545

26. Katiyar S, Singh D, Kumari S, Srivastava P, Mishra A. Novel strategies for designing regenerative skin products for accelerated wound healing. *3 Biotech.* 2022;12(11):316.

doi: 10.1007/s13205-022-03331-y

27. Deng X, Gould M, Ali MA. A review of current advancements for wound healing: Biomaterial applications and medical devices. *J Biomed Mater Res B Appl Biomater.* 2022;110(11):2542-2573.

doi: 10.1002/jbm.b.35086

28. Hama R, Reinhardt JW, Ulziibayar A, Watanabe T, Kelly J, Shinoka T. Recent Tissue Engineering Approaches to Mimicking the Extracellular Matrix Structure for Skin Regeneration. *Biomimetics.* 2023;8(1):130.

doi: 10.3390/biomimetics8010130

29. Rahmati M, Blaker JJ, Lyngstadaas SP, Mano JF, Haugen HJ. Designing multigradient biomaterials for skin regeneration. *Mater Today Adv.* 2020;5:100051.

doi: 10.1016/j.mtadv.2019.100051

30. Bruzauskaite I, Bironaite D, Bagdonas E, Bernotiene E. Scaffolds and cells for tissue regeneration: different scaffold pore sizes-different cell effects. *Cytotechnology.* 2016;68(3):355-369.

doi: 10.1007/s10616-015-9895-4

31. Gaharwar AK, Singh I, Khademhosseini A. Engineered biomaterials for in situ tissue regeneration. *Nat Rev Mater.* 2020;5(9):686-705.

doi: 10.1038/s41578-020-0209-x

32. Zhang M, Xing J, Zhong Y, Zhang T, Liu X, Xing D. Advanced function, design and application of skin substitutes for skin regeneration. *Mater Today Bio.* 2024;24:100918.

doi: 10.1016/j.mtbio.2023.100918

33. Wahlsten A, Stracuzzi A, Luchtefeld I, *et al*. Multiscale mechanical analysis of the elastic modulus of skin. *Acta Biomater.* 2023;170:155-168.

doi: 10.1016/j.actbio.2023.08.030

34. Espina JA, Marchant CL, Barriga EH. Durotaxis: the mechanical control of directed cell migration. *FEBS J.* 2022;289(10):2736-2754.

doi: 10.1111/febs.15862

35. Mamun AA, Shao C, Geng P, Wang S, Xiao J. Recent advances in molecular mechanisms of skin wound healing and its treatments. *Front Immunol.* 2024;15:1395479.

doi: 10.3389/fimmu.2024.1395479

36. Tottoli EM, Dorati R, Genta I, Chiesa E, Pisani S, Conti B. Skin Wound Healing Process and New Emerging Technologies for Skin Wound Care and Regeneration. *Pharmaceutics.* 2020;12(8):735.

doi: 10.3390/pharmaceutics12080735

37. Yang Y, Huang J, Zeng A, Long X, Yu N, Wang X. The role of the skin microbiome in wound healing. *Burns Trauma.* 2024;12:tkad059.

doi: 10.1093/burnst/tkad059

38. Moon S, Hong J, Go S, Kim BS. Immunomodulation for Tissue Repair and Regeneration. *Tissue Eng Regen Med.* 2023;20(3):389-409.

doi: 10.1007/s13770-023-00525-0

39. Yuqiang W, Ziyan Z, Xuedi S, Chengdong P. Recent progress in immunomodulation-based strategies for bone repair. *Regen Ther.* 2026;31:101054.

doi: 10.1016/j.reth.2025.101054

40. Chen S, Saeed A, Liu Q, *et al*. Macrophages in immunoregulation and therapeutics. *Signal Transduct Target Ther.* 2023;8(1):207.

doi: 10.1038/s41392-023-01452-1

41. Della Rocca Y, Fonticoli L, Rajan TS, *et al*. Hypoxia: molecular pathophysiological mechanisms in human diseases. *J Physiol Biochem.* 2022;78(4):739-752.

doi: 10.1007/s13105-022-00912-6

42. Hadjipanayi E, Schilling AF. Hypoxia-based strategies for angiogenic induction: the dawn of a new era for ischemia therapy and tissue regeneration. *Organogenesis.* 2013;9(4):261-272.

doi: 10.4161/org.25970

43. Moghanian A, Hosseini SH, Baino F, *et al*. Recent Advancements in Oxygen-Releasing Materials for Tissue Regenerative Medicine and Wound Healing. *Mater Today Commun.* 2026;50:114582.

doi: 10.1016/j.mtcomm.2025.114582

44. Shi Y, Guo S, Tian J, *et al*. Biomaterials-mediated sequential drug delivery: Emerging trends for wound healing. *Asian J Pharm Sci.* 2025;20(6):101088.

doi: 10.1016/j.ajps.2025.101088

45. Zhao X, Xu H, Sun Y, Yang Y, Guo B. Self-Adaptive Wound Dressings for Wound Healing and Repair. *Adv Mater.* 2026;38(29):e15854.

doi: 10.1002/adma.202515854

46. Chen Y, Shafiq M, Liu M, Morsi Y, Mo X. Advanced fabrication for electrospun three-dimensional nanofiber aerogels and scaffolds. *Bioact Mater.* 2020;5(4):963-979.

doi: 10.1016/j.bioactmat.2020.06.023

47. Kai D, Jin G, Prabhakaran MP, Ramakrishna S. Electrospun synthetic and natural nanofibers for regenerative medicine and stem cells. *Biotechnol J.* 2013;8(1):59-72.

doi: 10.1002/biot.201200249

48. Ma YQ, Zhou RY, Yang M, *et al*. Electrospinning-based bone tissue scaffold construction: Progress and trends. *Mater Des.* 2025;252:113792.

doi: 10.1016/j.matdes.2025.113792

49. Li J, Fischer P. Advances in extrusion-based bioprinting enabled by advanced printhead and nozzle designs. *Mater Today Bio.* 2026;37:102941.

doi: 10.1016/j.mtbio.2026.102941

50. Malekpour A, Chen X. Printability and Cell Viability in Extrusion-Based Bioprinting from Experimental, Computational, and Machine Learning Views. *J Funct Biomater.* 2022;13(2):40.

doi: 10.3390/jfb13020040

51. Schwab A, Levato R, D'Este M, Piluso S, Eglin D, Malda J. Printability and Shape Fidelity of Bioinks in 3D Bioprinting. *Chem Rev.* 2020;120(19):11028-11055.

doi: 10.1021/acs.chemrev.0c00084

52. Ng WL, Shkolnikov V. Optimizing cell deposition for inkjet-based bioprinting. *Int J Bioprint.* 2024;10(2):182-206.

doi: 10.36922/ijb.2135

53. Derakhshanfar S, Mbeleck R, Xu K, Zhang X, Zhong W, Xing M. 3D bioprinting for biomedical devices and tissue engineering: A review of recent trends and advances. *Bioact Mater.* 2018;3(2):144-156.

doi: 10.1016/j.bioactmat.2017.11.008

54. Afridi A, Al Rashid A, Koç M. Recent advances in the development of stereolithography-based additive manufacturing processes: A review of applications and challenges. *Bioprinting.* 2024;43:e00360.

doi: 10.1016/j.bprint.2024.e00360

55. Hu Y, Luo Z, Bao Y. Trends in Photopolymerization 3D Printing for Advanced Drug Delivery Applications. *Biomacromolecules.* 2025;26(1):85-117.

doi: 10.1021/acs.biomac.4c01004

56. Jeong YG, Yoo JJ, Lee SJ, Kim MS. 3D digital light process bioprinting: Cutting-edge platforms for resolution of organ fabrication. *Mater Today Bio.* 2024;29:101284.

doi: 10.1016/j.mtbio.2024.101284

57. Jiao T, Wang Z, Han G, Liu C, He C, Ma S. 3D Bioprinting for structural and functional skin regeneration: Technologies, bioinks, and key challenges. *Biointerphases.* 2026;21(1):010801.

doi: 10.1116/6.0004978

58. Yu K, Zhang X, Sun Y, *et al*. Printability during projection-based 3D bioprinting. *Bioact Mater.* 2022;11:254-267.

doi: 10.1016/j.bioactmat.2021.09.021

59. Swetha S, Sahiti TJ, Priya GS, Harshitha K, Anil A. Review on digital light processing (DLP) and effect of printing parameters on quality of print. *Interactions.* 2024;245(1):178.

doi: 10.1007/s10751-024-02018-5

60. Chaudhary R, Fabbri P, Leoni E, Mazzanti F, Akbari R, Antonini C. Additive manufacturing by digital light processing: a review. *Prog Addit Manuf.* 2023;8(2):331-351.

doi: 10.1007/s40964-022-00336-0

61. Mathur V, Agarwal P, Kasturi M, Srinivasan V, Seetharam RN, Vasanthan KS. Innovative bioinks for 3D bioprinting: Exploring technological potential and regulatory challenges. *J Tissue Eng.* 2025;16:20417314241308022.

doi: 10.1177/20417314241308022

62. Tong F, Zhang X, Wang X, *et al*. Digital Light Processing of Methacrylated Silk Fibroin Microneedles: Precision Engineering for Enhanced Transdermal Delivery and Skin Regeneration. *ACS Appl Bio Mater.* 2025;8(7):6025-6039.

doi: 10.1021/acsabm.5c00621

63. Fu C, Liu G, Fan Y, *et al*. Highly printable and multifunctional cell-laden collagen-based bioinks for precise DLP bioprinting and rapid diabetic wound regeneration. *Mater Today Bio.* 2025;32:101908.

doi: 10.1016/j.mtbio.2025.101908

64. Huh J, Moon YW, Park J, Atala A, Yoo JJ, Lee SJ. Combinations of photoinitiator and UV absorber for cell-based digital light processing (DLP) bioprinting. *Biofabrication.* 2021;13(3):034103.

doi: 10.1088/1758-5090/abfd7a

65. Calafel MI, Criado-Gonzalez M, Aguirresarobe R, Fernández M, Mijangos C. From rheological concepts to additive manufacturing assessment of hydrogel-based materials for advanced bioprinting applications. *Mater Adv.* 2025;6(14):4566-4597.

doi: 10.1039/d5ma00019j

66. Vazquez-Martel C, Becker L, Liebig WV, Elsner P, Blasco E. Vegetable Oils as Sustainable Inks for Additive Manufacturing: A Comparative Study. *ACS Sustainable Chem Eng.* 2021;9(49):16840-16848.

doi: 10.1021/acssuschemeng.1c06784

67. Wang XH, Liu JH, Dong RH, Gilchrist MD, Zhang N. High-precision digital light processing (DLP) printing

of microstructures for microfluidics applications based on a machine learning approach. *Virtual Phys Prototyp.* 2024;19(1):e2318774.

doi: 10.1080/17452759.2024.2318774

68. Lim KS, Galarraga JH, Cui X, Lindberg GCJ, Burdick JA, Woodfield TBF. Fundamentals and Applications of Photo-Cross-Linking in Bioprinting. *Chem Rev.* 2020;120(19):10662-10694.

doi: 10.1021/acs.chemrev.9b00812

69. You S, Wang P, Schimelman J, Hwang HH, Chen S. High-fidelity 3D Printing using Flashing Photopolymerization. *Addit Manuf.* 2019;30:100834.

doi: 10.1016/j.addma.2019.100834

70. Law ACC, Wang R, Chung J, *et al*. Process parameter optimization for reproducible fabrication of layer porosity quality of 3D-printed tissue scaffold. *J Intell Manuf.* 2024;35(4):1825-1844.

doi: 10.1007/s10845-023-02141-0

71. Li W, Hu X, Liu H, *et al*. 3D light-curing printing to construct versatile octopus-bionic patches. *J Mater Chem B.* 2023;11(22):5010-5020.

doi: 10.1039/d3tb00590a

72. Kumari S, Mondal P, Chatterjee K. Digital light processing-based 3D bioprinting of kappa-carrageenan hydrogels for engineering cell-loaded tissue scaffolds. *Carbohydr Polym.* 2022;290:119508.

doi: 10.1016/j.carbpol.2022.119508

73. Choi KY, Ajiteru O, Hong H, *et al*. A digital light processing 3D-printed artificial skin model and full-thickness wound models using silk fibroin bioink. *Acta Biomater.* 2023;164:159-174.

doi: 10.1016/j.actbio.2023.04.034

74. Nail A, Liu H, Meng DC, *et al*. 3D-printed insulin/GOx-loaded ZIF-8 microneedles via hydrogen-bond-enhanced photopolymerization for transdermal drug delivery. *Surfaces Interfaces.* 2025;72:107005.

doi: 10.1016/j.surfin.2025.107005

75. He XC, Chen XN, Liu YH, *et al*. A blue light 3D printable hydrogel with water absorption, antibacterial, and hemostatic properties for skin wound healing. *Chem Eng J.* 2024;493:152439.

doi: 10.1016/j.cej.2024.152439

76. Yang XX, Yao LY, Sun XX, Wang LL, Xiao JX. Low-temperature DLP 3D printing of low-concentration collagen methacryloyl for the fabrication of durable and bioactive personalized scaffolds. *Chem Eng J.* 2024;497:155650.

doi: 10.1016/j.cej.2024.155650

77. Wang Y, Li Y, Zhou H, *et al*. Innovations in theoretical modeling for vat photopolymerization. *Mater Des.* 2026;262:115384.

doi: 10.1016/j.matdes.2025.115384

78. Kolibaba TJ, Killgore JP, Caplins BW, *et al*. Results of an interlaboratory study on the working curve in vat photopolymerization. *Addit Manuf.* 2024;84:104082.

doi: 10.1016/j.addma.2024.104082

79. Shahzadi L. *New chemical resins for SLA-based 3D printers*. Thesis. Hobart, Australia: University of Tasmania; 2022.

80. Li Y, Mao QJ, Yin J, Wang YF, Fu JZ, Huang Y. Theoretical prediction and experimental validation of the digital light processing (DLP) working curve for photocurable materials. *Addit Manuf.* 2021;37:101716.

doi: 10.1016/j.addma.2020.101716

81. Hofstetter C, Orman S, Baudis S, Stampfl J. Combining cure depth and cure degree, a new way to fully characterize novel photopolymers. *Addit Manuf.* 2018;24:166-172.

doi: 10.1016/j.addma.2018.09.025

82. Arias-Ferreiro G, Ares-Pernas A, Lasagabaster-Latorre A, *et al*. Printability Study of a Conductive Polyaniline/Acrylic Formulation for 3D Printing. *Polymers.* 2021;13(13):2068.

doi: 10.3390/polym13132068

83. Caplins BW, Kolibaba TJ, Arp U, *et al*. Influence of Spectral Bandwidth on the Working Curve in Vat Photopolymerization. *Addit Manuf.* 2024;85:104172.

doi: 10.1016/j.addma.2024.104172

84. Billerbeck K, Hägele C, Träger J. Relation of the working curve and exposure intensity in VPP 3D-printing. *Prog Addit Manuf.* 2024;9(4):1015-1023.

doi: 10.1007/s40964-023-00498-5

85. Gladush GG, Smurov I. *Physics of Laser Materials Processing: Theory and Experiment*. Vol 146. Berlin, Germany: Springer Science & Business Media; 2011.

86. Steudel F, Lisec T, Nolte PW, *et al*. Pixelated phosphors for high-resolution and high-contrast white light sources: erratum. *Opt Express.* 2019;27(6):9097-9098.

doi: 10.1364/OE.27.009097

87. Seeboth A, Lötzsch D, Potechius E. Phase transitions and phase separations in aqueous polyether systems. *Colloid Polym Sci.* 2001;279(7):696-704.

doi: 10.1007/s003960000474

88. Auger JC, Barrera RG, Stout B. Scattering efficiency of clusters composed by aggregated spheres. *J Quant Spectrosc Radiat Transf.* 2003;79:521-531.

doi: 10.1016/S0022-4073(02)00305-9

89. Sun Y, Yu K, Nie J, *et al*. Modeling the printability of photocuring and strength adjustable hydrogel bioink during projection-

based 3D bioprinting. *Biofabrication.* 2021;13(3):035032.

doi: 10.1088/1758-5090/aba413

90. Li Y, Mao QJ, Li XK, *et al*. High-fidelity and high-efficiency additive manufacturing using tunable pre-curing digital light processing. *Addit Manuf.* 2019;30:100889.

doi: 10.1016/j.addma.2019.100889

91. Escobar ICP, Chaves L, Paula CTB, Pereira P, Serra AC, Coelho JFJ. Development of a Tunable Dextran-PCL Biomaterial Photoink for High-Resolution DLP 3D Printing in Biomedical Applications. *ACS Appl Mater Interfaces.* 2025;17(46):63272-63285.

doi: 10.1021/acsami.5c18856

92. Quan H, Zhang T, Xu H, Luo S, Nie J, Zhu X. Photo-curing 3D printing technique and its challenges. *Bioact Mater.* 2020;5(1):110-115.

doi: 10.1016/j.bioactmat.2019.12.003

93. Garciamendez-Mijares CE, Aguilar FJ, Hernandez P, *et al*. Design considerations for digital light processing bioprinters. *Appl Phys Rev.* 2024;11(3):031314.

doi: 10.1063/5.0187558

94. Guerra AJ, Lammel-Lindemann J, Katko A, *et al*. Optimization of photocrosslinkable resin components and 3D printing process parameters. *Acta Biomater.* 2019;97:154-161.

doi: 10.1016/j.actbio.2019.07.045

95. Sherman SL, Kadioglu O, Currier GF, Kierl JP, Li J. Accuracy of digital light processing printing of 3-dimensional dental models. *Am J Orthod Dentofacial Orthop.* 2020;157(3):422-428.

doi: 10.1016/j.ajodo.2019.10.012

96. Das S, Jegadeesan JT, Basu B. Gelatin Methacryloyl (GelMA)-Based Biomaterial Inks: Process Science for 3D/4D Printing and Current Status. *Biomacromolecules.* 2024;25(4):2156-2221.

doi: 10.1021/acs.biomac.3c01271

97. Pagac M, Hajnys J, Ma QP, *et al*. A Review of Vat Photopolymerization Technology: Materials, Applications, Challenges, and Future Trends of 3D Printing. *Polymers.* 2021;13(4):598.

doi: 10.3390/polym13040598

98. Hakim Khalili M, Zhang R, Wilson S, Goel S, Impey SA, Aria AI. Additive Manufacturing and Physicomechanical Characteristics of PEGDA Hydrogels: Recent Advances and Perspective for Tissue Engineering. *Polymers.* 2023;15(10):2341.

doi: 10.3390/polym15102341

99. Lim J, Bupphathong S, Huang W, Lin CH. Three-Dimensional Bioprinting of Biocompatible Photosensitive Polymers for Tissue Engineering Application. *Tissue Eng Part B Rev.* 2023;29(6):710-722.

doi: 10.1089/ten.TEB.2023.0072

100. Uysal E. *Development of Biocompatible and Flexible Polymers for DLP Processing and Improvement of Mechanical Properties*. PhD Thesis. Istanbul, Turkey: Marmara Universitesi; 2021.

101. Azani MR, Hassanpour A. UV-Curable Polymer Nanocomposites: Material Selection, Formulations, and Recent Advances. *J Compos Sci.* 2024;8(11):441.

doi: 10.3390/jcs8110441

102. Kim M, Kang D, Han H, Jang J. Light-activated decellularized extracellular matrix-based bioinks for enhanced mechanical integrity. *Mater Today Bio.* 2025;32:101859.

doi: 10.1016/j.mtbio.2025.101859

103. Wu Q, Chauhan M, Khamaisi B, Nassar-Marjiya E, Farah S. Biomimetic 3D-Printed Adaptive Hydrogel Bioadhesives Featuring Superior Infection Resistance for Challenging Tissue Adhesion, Hemostasis, and Healthcare. *Adv Mater.* 2025;37(44):e2502850.

doi: 10.1002/adma.202502850

104. Silva R, Medeiros M, Paula CTB, *et al*. Light-Mediated 3D-Printed Wound Dressings Based on Natural Polymers with Improved Adhesion and Antioxidant Properties. *Polymers.* 2025;17(8):1114.

doi: 10.3390/polym17081114

105. Wu Z, Liu J, Lin J, *et al*. Novel Digital Light Processing Printing Strategy Using a Collagen-Based Bioink with Prospective Cross-Linker Procyanidins. *Biomacromolecules.* 2022;23(1):240-252.

doi: 10.1021/acs.biomac.1c01244

106. Chen D, Sun L, Wang J, *et al*. Carboxymethyl chitosan microneedles patch with tunable stiffness regulates wound scar-free repair. *J Biomech.* 2025;189:112846.

doi: 10.1016/j.jbiomech.2025.112846

107. Ghosh S, Pati F. Decellularized extracellular matrix and silk fibroin-based hybrid biomaterials: A comprehensive review on fabrication techniques and tissue-specific applications. *Int J Biol Macromol.* 2023;253(Pt 8):127410.

doi: 10.1016/j.ijbiomac.2023.127410

108. Vernengo AJ, Grad S, Eglin D, Alini M, Li Z. Bioprinting Tissue Analogues with Decellularized Extracellular Matrix Bioink for Regeneration and Tissue Models of Cartilage and Intervertebral Discs. *Adv Funct Mater.* 2020;30(44):1909044.

doi: 10.1002/adfm.201909044

109. Hewawasam RS, Blomberg R, Serbedzija P, Magin CM. Chemical Modification of Human Decellularized Extracellular Matrix for Incorporation into Phototunable Hybrid-Hydrogel Models of Tissue Fibrosis. *ACS Appl*

Mater Interfaces. 2023;15(12):15071-15083.

doi: 10.1021/acsami.2c18330

110. Loh JM, Lim YJL, Tay JT, Cheng HM, Tey HL, Liang K. Design and fabrication of customizable microneedles enabled by 3D printing for biomedical applications. *Bioact Mater.* 2024;32:222-241.

doi: 10.1016/j.bioactmat.2023.09.022

111. Zhu Q, Zhou X, Zhang Y, *et al*. White-light crosslinkable milk protein bioadhesive with ultrafast gelation for first-aid wound treatment. *Biomater Res.* 2023;27(1):6.

doi: 10.1186/s40824-023-00346-1

112. Chen S, Xiong Y, Yang F, *et al*. Approaches to scarless burn wound healing: application of 3D printed skin substitutes with dual properties of anti-infection and balancing wound hydration levels. *EBioMedicine.* 2024;106:105258.

doi: 10.1016/j.ebiom.2024.105258

113. Vyas J, Raytthatha N, Vyas P, *et al*. Biomaterial-Based Additive Manufactured Composite/Scaffolds for Tissue Engineering and Regenerative Medicine: A Comprehensive Review. *Polymers.* 2025;17(8):1090.

doi: 10.3390/polym17081090

114. Zheng L, Tseomashko N, Voronova A, Vasil'kov A, Hu XQ, Wang XY. Recent advances of collagen composite biomaterials for biomedical engineering: antibacterial functionalization and 3D-printed architecturalization. *Collagen Leather.* 2024;6(1):22.

doi: 10.1186/s42825-024-00164-8

115. Li M, Sun L, Liu Z, *et al*. 3D bioprinting of heterogeneous tissue-engineered skin containing human dermal fibroblasts and keratinocytes. *Biomater Sci.* 2023;11(7):2461-2477.

doi: 10.1039/d2bm02092k

116. Shan J, Che J, Song C, Zhao Y. Emerging antibacterial nanozymes for wound healing. *Smart Med.* 2023;2(3):e20220025.

doi: 10.1002/SMMD.20220025

117. Shariatzadeh FJ, Currie S, Logsetty S, Spiwak R, Liu S. Enhancing wound healing and minimizing scarring: A comprehensive review of nanofiber technology in wound dressings. *Prog Mater Sci.* 2025;147:101350.

doi: 10.1016/j.pmatsci.2024.101350

118. Zhang L, Song Q, Yang P, Liu Z. HAMA/GelMA-based hydrogel microneedle patch via DLP 3D bioprinting for high-efficiency ISF extraction. *Int J Pharm.* 2025;680:125800.

doi: 10.1016/j.ijpharm.2025.125800

119. Lin DM, Li MQ, Wang LL, *et al*. Multifunctional Hydrogel Based on Silk Fibroin Promotes Tissue Repair and Regeneration. *Adv Funct Mater.* 2024;34(39):2405255.

doi: 10.1002/adfm.202405255

120. Zhu J, Zhou H, Gerhard EM, *et al*. Smart bioadhesives for wound healing and closure. *Bioact Mater.* 2023;19:360-375.

doi: 10.1016/j.bioactmat.2022.04.020

121. Hou CS, Yi B, Yao X. Revolutionizing Bioadhesives With Intelligent Technologies: Toward Precision and Smart Control. *Adv Funct Mater.* 2026;36(47):e32185.

doi: 10.1002/adfm.202532185

122. Lu Z, Cui J, Liu F, *et al*. A 4D Printed Adhesive, Thermo-Contractile, and Degradable Hydrogel for Diabetic Wound Healing. *Adv Healthc Mater.* 2024;13(10):e2303499.

doi: 10.1002/adhm.202303499

123. Saha RK, Hassan M, Ali MR, Islam MM, Das A. Advancements in Sustainable Bioprinting: Materials, Challenges and Opportunities in Transition from 3D to 4D Printing. *Biomed Eng Adv.* 2026;11:100216.

doi: 10.1016/j.bea.2026.100216

124. Yucer S, Sarac B, Ciftci F. Bioprinting revolution: Innovative design of 3D bioactive scaffolds for living organs and transdermal tissues. *Bioeng Transl Med.* 2025;10(6):e70080.

doi: 10.1002/btm2.70080

125. Eming SA, Martin P, Tomic-Canic M. Wound repair and regeneration: mechanisms, signaling, and translation. *Sci Transl Med.* 2014;6(265):265sr6.

doi: 10.1126/scitranslmed.3009337

126. Frykberg RG, Banks J. Challenges in the Treatment of Chronic Wounds. *Adv Wound Care.* 2015;4(9):560-582.

doi: 10.1089/wound.2015.0635

127. Yao H, Jing SL, Huang KX, *et al*. Clinical Features and Mechanisms of Differential Wound Healing and Scarring Across Anatomical Sites. *Adv Wound Care.* 2026;15(8):580-595.

doi: 10.1177/21621918251387627

128. Xiao J, Dai X, An X, *et al*. Precision Strategies for Enhanced Chronic Skin Wound Healing Using Multifunctional Hydrogels. *Precis Med Eng.* 2025;3(1):100054.

doi: 10.1016/j.preme.2025.100054

129. Liu H, Nail A, Meng D, *et al*. Bioinspired 3D-Printed NIR-Responsive MXene-Based Multifunctional Eutectogel Microneedles for Personalized Infected Wound Healing. *Adv Healthc Mater.* 2026;14(16):e2501344.

doi: 10.1002/adhm.202501344

130. Pfalzgraff A, Brandenburg K, Weindl G. Antimicrobial Peptides and Their Therapeutic Potential for Bacterial Skin Infections and Wounds. *Front Pharmacol.* 2018;9:281.

doi: 10.3389/fphar.2018.00281

131. Park J, Kim J, Fakhraei Lahiji S, Kim YH. Dual-Phase Antibacterial and Anti-inflammatory Self-Locking

Microarray Patches for the Effective Treatment of Acne Vulgaris. *ACS Appl Mater Interfaces.* 2025;17(32):45438-45447.

doi: 10.1021/acsami.5c07718

132. Chen Y, Wang C, Zhang Z, *et al.* 3D-printed piezocatalytic hydrogels for effective antibacterial treatment of infected wounds. *Int J Biol Macromol.* 2024;268(Pt 2):131637.

doi: 10.1016/j.ijbiomac.2024.131637

133. Tao J, Xu X, Wang S, *et al.* Polydiacetylene-Nanoparticle-Functionalized Microgels for Topical Bacterial Infection Treatment. *ACS Macro Lett.* 2019;8(5):563-568.

doi: 10.1021/acsmacrolett.9b00196

134. Chen Z, Wang Y, Kai Y, *et al.* Vine Tea Combined with a Lidocaine Microneedle Patch for Enhanced Treatment of Psoriasis. *ACS Omega.* 2025;10(43):50904-50913.

doi: 10.1021/acsomega.5c03831

135. Wang L, Yang K, Xie XX, *et al.* Macrophages as Multifaceted Orchestrators of Tissue Repair: Bridging Inflammation, Regeneration, and Therapeutic Innovation. *J Inflamm Res.* 2025;18:8945-8959.

doi: 10.2147/Jir.S527764

136. Schilrreff P, Alexiev U. Chronic Inflammation in Non-Healing Skin Wounds and Promising Natural Bioactive Compounds Treatment. *Int J Mol Sci.* 2022;23(9):4928.

doi: 10.3390/ijms23094928

137. Yan L, Wang J, Cai X, *et al.* Macrophage plasticity: signaling pathways, tissue repair, and regeneration. *MedComm.* 2024;5(8):e658.

doi: 10.1002/mco2.658

138. Mantovani A, Biswas SK, Galdiero MR, Sica A, Locati M. Macrophage plasticity and polarization in tissue repair and remodelling. *J Pathol.* 2013;229(2):176-185.

doi: 10.1002/path.4133

139. Lee J, Dutta SD, Acharya R, *et al.* Stimuli-Responsive 3D Printable Conductive Hydrogel: A Step toward Regulating Macrophage Polarization and Wound Healing. *Adv Healthc Mater.* 2024;13(4):e2302394.

doi: 10.1002/adhm.202302394

140. Shahin H, Elmasry M, Steinvall I, Söberg F, El-Serafi A. Vascularization is the next challenge for skin tissue engineering as a solution for burn management. *Burns Trauma.* 2020;8:tkaa022.

doi: 10.1093/burnst/tkaa022

141. Amirsadeghi A, Jafari A, Eggermont LJ, Hashemi SS, Bencherif SA, Khorram M. Vascularization strategies for skin tissue engineering. *Biomater Sci.* 2020;8(15):4073-4094.

doi: 10.1039/d0bm00266f

142. Zhou F, Hong Y, Liang R, *et al.* Rapid printing of bio-inspired 3D tissue constructs for skin regeneration. *Biomaterials.* 2020;258:120287.

doi: 10.1016/j.biomaterials.2020.120287

143. Mazari-Arrighi E, Lepine M, Ayollo D, *et al.* Self-Organization of Long-Lasting Human Endothelial Capillary-Like Networks Guided by DLP Bioprinting. *Adv Healthc Mater.* 2024;13(14):e2302830.

doi: 10.1002/adhm.202302830

144. Saghazadeh S, Rinoldi C, Schot M, *et al.* Drug delivery systems and materials for wound healing applications. *Adv Drug Deliv Rev.* 2018;127:138-166.

doi: 10.1016/j.addr.2018.04.008

145. Liu YH, He CF, Qiao TH, *et al.* Coral-Inspired Hollow Microneedle Patch with Smart Sensor Therapy for Wound Infection. *Adv Funct Mater.* 2024;34(24):2314071.

doi: 10.1002/adfm.202314071

146. Li B, Wu T, Liu B, *et al.* Digital light processing-printed personalized gelatin Methacryloyl/silk fibroin Methacryloyl hydrogel microneedles loaded with platelet-rich proteins for accelerated wound healing. *Int J Biol Macromol.* 2025;316(Pt 1):144693.

doi: 10.1016/j.ijbiomac.2025.144693

147. Fang ZX, Lin L, Li ZQ, *et al.* Stimuli-responsive heparin-drug conjugates co-assembled into stable nanomedicines for cancer therapy. *Acta Biomater.* 2023;164:422-434.

doi: 10.1016/j.actbio.2023.04.016

148. Joshi A, Kaur T, Joshi A, Gugulothu SB, Choudhury S, Singh N. Light-Mediated 3D Printing of Micro-Pyramid-Decorated Tailorable Wound Dressings with Endogenous Growth Factor Sequestration for Improved Wound Healing. *ACS Appl Mater Interfaces.* 2023;15(1):327-337.

doi: 10.1021/acsami.2c16418

149. Yun M, Langford L, Russell L, Ndiforamang N, Zhang A, Bai W. Emerging stimuli-responsive hydrogels for enhancing chronic wound healing. *RSC Appl Polym.* 2026;4(1):53-82.

doi: 10.1039/d5lp00092k

150. Hama R, Aytemiz D, Moseti KO, Kameda T, Nakazawa Y. Silk Fibroin Conjugated with Heparin Promotes Epithelialization and Wound Healing. *Polymers.* 2022;14(17):3582.

doi: 10.3390/polym14173582

151. Sun YZ, Wang XC, Tang M, *et al.* 3D Printing of Succulent-Inspired Microneedle Array for Enhanced Tissue Adhesion and Controllable Drug Release. *Adv Mater Technol.* 2024;9(15):2400216.

doi: 10.1002/admt.202400216

152. Guo S, Cui H, Agarwal T, Zhang LG. Nanomaterials in 4D Printing: Expanding the Frontiers of Advanced

Manufacturing. *Small.* 2024;20(30):e2307750.

doi: 10.1002/smll.202307750

153. Ding L, Shangguan H, Tu H, *et al.* Multi-Stimulus-Responsive Smart Hydrogels: Response Mechanisms, Synthesis Strategies, and Frontiers in Biomedical Applications. *ACS Biomater Sci Eng.* 2026;12(4):2045-2078.

doi: 10.1021/acsbiomaterials.5c02155

154. Yang S, Zhang W, Gao L, *et al.* Customizable glucose-responsive gelatin methacryloyl-based hydrogel microneedle patches for antibacterial therapy and promoted diabetic wound healing. *Int J Biol Macromol.* 2025;332(Pt 2):148610.

doi: 10.1016/j.ijbiomac.2025.148610

155. Umur E, Bayrak E, Arslan F, *et al.* Advances in Three Dimensional Bioprinting for Wound Healing: A Comprehensive Review. *Appl Sci.* 2023;13(18):10269.

doi: 10.3390/app131810269

156. Zhu Z, Wang J, Pei X, *et al.* Blue-ringed octopus-inspired microneedle patch for robust tissue surface adhesion and active injection drug delivery. *Sci Adv.* 2023;9(25):eadh2213.

doi: 10.1126/sciadv.adh2213

157. Makvandi P, Maleki A, Shabani M, *et al.* Bioinspired microneedle patches: Biomimetic designs, fabrication, and biomedical applications. *Matter.* 2022;5(2):390-429.

doi: 10.1016/j.matt.2021.11.021

158. Baik S, Lee HJ, Kim DW, Kim JW, Lee Y, Pang C. Bioinspired Adhesive Architectures: From Skin Patch to Integrated Bioelectronics. *Adv Mater.* 2019;31(34):e1803309.

doi: 10.1002/adma.201803309

159. Ma H, Liu Z, Lu X, *et al.* 3D printed multi-coupled bioinspired skin-electronic interfaces with enhanced adhesion for monitoring and treatment. *Acta Biomater.* 2024;187:183-198.

doi: 10.1016/j.actbio.2024.08.048

160. Yang ZR, Yang XQ, Du KH, *et al.* Advancements in hemostatic and bioactive materials for full-course wound management: From hemostasis to scar prevention. *Mater Today Adv.* 2026;30:100812.

doi: 10.1016/j.mtadv.2026.100812

161. Kim H, Kang B, Cui XL, *et al.* Light-Activated Decellularized Extracellular Matrix-Based Bioinks for Volumetric Tissue Analogs at the Centimeter Scale. *Adv Funct Mater.* 2021;31(32):2011252.

doi: 10.1002/adfm.202011252

162. Bedir T, Baykara D, Yildirim R, *et al.* Three-Dimensional-Printed GelMA-KerMA Composite Patches as an Innovative Platform for Potential Tissue Engineering of Tympanic Membrane Perforations. *Nanomaterials.* 2024;14(7):563.

doi: 10.3390/nano14070563

163. Tabatabaei Rezaei N, Kumar H, Liu H, *et al.* Bioprinting of hepatic tissue model using photocrosslinkable dECM-containing composite hydrogel. *Mater Today Bio.* 2025;32:101824.

doi: 10.1016/j.mtbio.2025.101824

164. Jindal S, Bisharat M, Khamaisi B, *et al.* Biofilm-Antagonist Ginger-Based 3D-Printable Photoresins for Complex Implant Designs Exhibiting Advanced Multifunctional Biomedical Applications. *Adv Mater.* 2026;38(15):e03351.

doi: 10.1002/adma.202503351

165. Fan Y, Fu C, Wang J, *et al.* Zinc-enhanced methacrylated collagen bioinks with dual crosslinking for high-resolution DLP bioprinting of personalized anti-aging skin therapy. *Int J Biol Macromol.* 2025;330(Pt 4):148163.

doi: 10.1016/j.ijbiomac.2025.148163

166. Chansoria P, Chaudhari A, Etter EL, *et al.* Instantly adhesive and ultra-elastic patches for dynamic organ and wound repair. *Nat Commun.* 2024;15(1):4720.

doi: 10.1038/s41467-024-48980-0

167. Hu Y, Tang H, Xu N, *et al.* Adhesive, Flexible, and Fast Degradable 3D-Printed Wound Dressings with a Simple Composition. *Adv Healthc Mater.* 2024;13(3):e2302063.

doi: 10.1002/adhm.202302063

168. Yao C, Zhao Y, Wu Y, *et al.* Single-Doped W18O49-x@ Au-Embedded Dual-Network Silk Fibroin Hydrogel for NIR-Responsive Phototherapeutic Wound Healing. *Adv Healthc Mater.* 2026;15(7):e03108.

doi: 10.1002/adhm.202503108

169. Amara H, Alam F, El Turk S, Butt H. 3D-printed and In-situ prepared hydrogel anti-bacterial wound patch with silver nanoparticle embedded matrix. *Heliyon.* 2025;11(4):e42186.

doi: 10.1016/j.heliyon.2025.e42186

170. Fu C, Fan Y, Wang J, *et al.* Development of a Dual-Cross-Linked Collagen-Based Bioink for High-Resolution 3D Bioprinting and Antiaging. *Biomacromolecules.* 2026;27(1):309-321.

doi: 10.1021/acs.biomac.5c01416

171. Lin YH, Liu EW, Lin YJ, Ng HY, Lee JJ, Hsu TT. The Synergistic Effect of Electrical Stimulation and Dermal Fibroblast Cells-Laden 3D Conductive Hydrogel for Full-Thickness Wound Healing. *Int J Mol Sci.* 2023;24(14):11698.

doi: 10.3390/ijms241411698